ZEROTH ORDER RESONATOR (ZOR) BASED RFID ANTENNA DESIGN

A Dissertation
Submitted to the Graduate Faculty
of the
North Dakota State University
of Agriculture and Applied Science

By

Muhammad Mubeen Masud

In Partial Fulfillment
for the Degree of
DOCTOR OF PHILOSOPHY

Major Department:
Electrical and Computer Engineering

August 2014

Fargo, North Dakota

North Dakota State University
Graduate School

Title

ZEROTH ORDER RESONATOR (ZOR) BASED RFID ANTENNA DESIGN

By

Muhammad Mubeen Masud

The Supervisory Committee certifies that this ***disquisition*** complies with North Dakota State University's regulations and meets the accepted standards for the degree of

DOCTOR OF PHILOSOPHY

SUPERVISORY COMMITTEE:

Dr. Benjamin D. Braaten
Chair

Dr. David A. Rogers

Dr. Ivan T. Lima

Dr. Mijia Yang

Approved:

August 06, 2014
Date

Dr. Scott C. Smith
Department Chair

ABSTRACT

Meander-line and multi-layer antennas have been used extensively to design compact UHF radio frequency identification (RFID) tags; however the overall size reduction of meander-line antennas is limited by the amount of parasitic inductance that can be introduced by each meander-line segment, and multi-layer antennas can be too costly. In this study, a new compact antenna topology for passive UHF RFID tags based on zeroth order resonant (ZOR) design techniques is presented. The antenna consists of lossy coplanar conductors and either inter-connected inter-digital capacitor (IDC) or shunt inductor unit-cells with a ZOR frequency near the operating frequency of the antenna. Setting the ZOR frequency near the operating frequency is a key component in the design process because the unit-cells chosen for the design are inductive at the operating frequency. This makes the unit-cells very useful for antenna miniaturization. These new designs in this work have several benefits: the coplanar layout can be printed on a single layer, matching inductive loops that reduce antenna efficiency are not required and ZOR analysis can be used for the design. Finally, for validation, prototype antennas are designed, fabricated and tested.

ACKNOWLEDGMENTS

I am very grateful to take this opportunity to thank Dr. Benjamin D. Braaten, Dr. David A. Rogers, Dr. Ivan T. Lima, Dr. Mijia Yang and Dr. Orven F. Swenson for serving on my graduate committee. I cannot thank Dr. Benjamin D. Braaten enough for the guidance, encouragement and wisdom he gave me during my graduate studies. I always had the freedom to follow my own ideas for which I am very grateful. I would especially like to thank Dr. David A. Rogers and Dr. Ivan T. Lima. I really enjoyed working with you and learned a lot during this process.

I would like to thank Dr. Mijia Yang showing willingness to serve on my committee with such a short notice.

Finally, I would like to thank my family for their support and understanding in allowing me to leave my hometown to pursue this work.

DEDICATION

To my wife, son, mother, brother, sister and to all my friends for their endless love, support and encouragement throughout my career.

TABLE OF CONTENTS

LIST OF FIGURES

LIST OF SYMBOLS

ϵ ..... Permittivity

μ ..... Permeability

$\vec{k}$ ..... Wave number

$\vec{S}$ ..... Poynting vector in the direction of energy flow

$\vec{E}$ ..... Electric field

$\vec{H}$ ..... Magnetic field

λ ..... Wave length

c ..... Velocity of light

Z_a ..... Antenna impedance

$Z_{c_{1,2}}$ ..... RFID IC impedance in state 1 & 2

V_a ..... Voltage generated at the terminals of antenna

P_r ..... Received power

P_t ..... Transmitted power

G_t ..... Gain of transmitter antenna

G_r ..... Gain of receiver antenna

R ..... distance between transmitter and receiver

q ..... Impedance mismatch

p ..... Period of unit cell

β ..... Phase constant

L_R ..... Right handed inductance

L_L ..... Left handed inductance

C_R ..... Right handed capacitance

C_L ..... Left handed capacitance

Q ..... Quality factor

v_p ..... Phase velocity

ϵ_r ..... Relative permittivity

Z_0 ..... Characteristic impedance

t ..... Thickness of conductor

h ..... Height of substrate

α_c ..... Attenuation constant due to conductor

α_d ..... Attenuation constant due to dielectric

$\tan\delta$ ..... Loss tangent

α_{cpw} ..... Attenuation constant on host TL

β_{cpw} ..... Phase constant on host TL

Z_B ..... Bloch impedance

γ_{cpw} ..... Complex propagation constant on host TL

ω ..... Angular frequency

f_w ..... Finger width in IDC unit cell

f_g ..... Finger gap in IDC unit cell

σ ..... Conductivity

CHAPTER 1. INTRODUCTION

1.1. Introduction to Radio Frequency Identification (RFID)

Since its first use in the 1930s when it was used as IFF (Identify Friend or Foe) by the British allies to identify whether airplanes were friend or foe, radio frequency identification (RFID) has evolved and transformed into mainstream consumer goods identification and tracking applications. Being superior to the earlier used bar code technology, which requires not only a clear line of sight but also is limited to a small operational distance between the object and the scanner for identification purpose, RFID enables identification from a far greater distance, and also no line of sight is required for its successful operation [1]. These characteristics of RFID systems have made them more attractive and recently they have found applications in medicine, textiles, vehicle security, musical instruments, inventory control, tracking of products in a retail supply chain and managing large volumes of books in libraries [2–7].

The demand for more compact antennas on wireless devices is increasing steadily. This is especially noticeable for passive radio frequency identification (RFID) systems in the UHF band. Current RFID tags are much more compact than some of the original prototype RFID tags. This is because much research and development has been conducted on novel techniques, such as meander-lines [8] and multi-layer structures [9] to reduce the overall size of the antenna on a passive RFID tag. However, the size reduction of meander-line antennas is limited in part by the amount of parasitic inductance that can be introduced by the meander-line segments [10] and a multilayer antenna can make an RFID tag too costly.

1.2. Introduction to Metamaterials

Metamaterials (MTMs) are materials typically engineered with novel or artificial structures to produce electromagnetic properties that are unusual or difficult to obtain in nature. Because of their promise to provide engineerable permittivity ϵ,

permeability μ and index of refraction, metamaterials have drawn broad interest and have led to possible utilization in many electromagnetic applications from the microwave to optical regime, especially for the radiated-wave devices, for example in antenna designs due to their unique electromagnetic properties, such as anti-parallel phase and group velocities and zero propagation constant at a non-zero frequency [11–15].

1.2.1. Literature Review and Methodology

Before proceeding further it is essential to briefly explain the origin of the word metamaterial and its definition. There have been many definitions for metamaterial, they can be defined as class of "artificial" media, which exhibit extraordinary electromagnetic properties that are not found in nature. The word metamaterial is a derived word from Greek. Meta means "beyond" or "higher". That is metamaterials can have their electromagnetic properties altered to something beyond the electromagnetic properties of conventional materials which are found in nature.

Metamaterials refers to an artificial periodic media, for which the periodicity is a fraction of the wavelength of the incident electromagnetic wave [16]. Metamaterial derives its properties from its structure rather than its composition.

About the methodology, all the antenna simulations results are carried out by using Ansoft High Frequency Structural Simulator (HFSS) and Equivalent Circuit analysis is carried out in the Agilant Advance Design System (ADS).

1.2.2. Veselago and the Left-Handed Medium (LHM)

In the 1960s, Victor Georgievich Veselago, a Russian physicist, proposed that materials with simultaneously negative permittivity ϵ and permeability μ are physically permissible and possess a negative index of refraction. He concluded that such media is allowed by Maxwell's equations and that plane waves propagating inside them could be described by an electric field intensity vector $\vec{E}$, magnetic field

intensity vector $\vec{H}$, and wavevector $\vec{k}$. Veselago termed these left-handed media (LHM) because the vectors $\vec{E}$, $\vec{H}$, and $\vec{k}$ would form a left-handed triplet unlike a right-handed triplet which it forms in conventional right-handed media (RHM) [11]. The two arrangements are shown in Figure 1. Moreover, although $\vec{E}$, $\vec{H}$, and $\vec{k}$ form a left-handed triplet, $\vec{E}$,$\vec{H}$, and the Poynting vector $\vec{S}$ still maintains a right-handed relationship. Thus, in LHM the wavevector $\vec{k}$ is anti-parallel to the Poynting vector $\vec{S}$ and, although the energy still travels outwards from source, the phase is advanced rather than delayed in that direction.

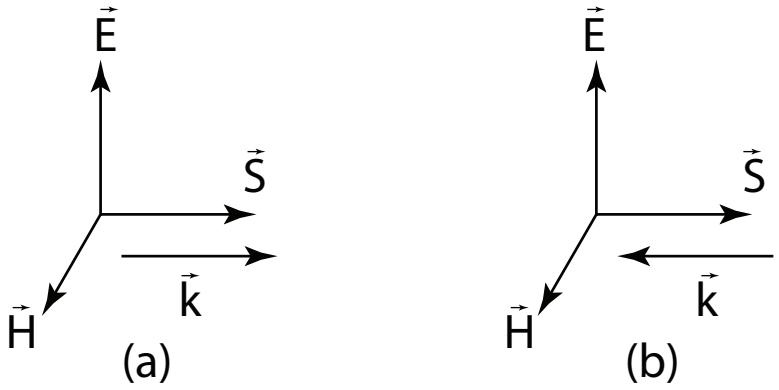

Figure 1. Orientation of fields $\vec{E}$, $\vec{H}$, $\vec{S}$ and $\vec{k}$ (a) Right-Handed Medium and (b) Left-Handed Medium.

1.3. Background and Scope of the Thesis

Primary research in metamaterial investigates material with a negative refractive index (NRI), which means material will exhibits both negative permittivity ϵ and permeability μ simultaneously, thus leading to a negative refractive index. There are two requirements to achieve an NRI value of refraction. First is to fabricate a material which can produce negative permeability $\mu_{eff} < 0$. Second, negative values for both permeability ϵ and permittivity μ must occur simultaneously over a common range of frequencies.

For obtaining both negative permeability and permittivity simultaneously, some resonance must be present [17]. The first negative refractive index or left handed media (LHM) was realized by using a periodic array of thin wires to synthesize negative permittivity and split ring resonators (SRRs) to synthesize a negative permeability [18–20]. Later on another method was developed to realize NRI or left handed media, called the transmission line method (TL). In this method, a transmission line is periodically loaded with series capacitors and shunt inductors to obtain an NRI.

Metamaterial (MTM) technologies can be used to design and develop radio frequency (RF) components and subsystems with a performance similar to or exceeding conventional RF structures, at a fraction of existing sizes; with antenna size reduction as much as $\lambda/40$. The techniques can be used to identify suitable structures that are low-cost and easy to manufacture while maintaining high efficiency, gain and compact sizes. One limitation of various MTM antennas and resonators is a narrow bandwidth around a resonating frequency in either single-band or multi-band antennas. There have been a number of studies that have investigated how to enhance the bandwidth of Zeroth-Order Resonant (ZOR) antennas [21–24].

In this thesis, ZOR based RFID antenna is proposed with a host coplanar waveguide (CPW) TL. The equivalent circuit of the antenna is extracted and the corresponding propagation characteristic analysis is performed in ADS.

1.4. Motivation

The challenges facing next generation wireless communication systems are multifaceted. On the one hand there is a trend towards the miniaturization of components associated with handheld devices such as laptops, mobile phones, PDA's and GPS's, but on the other hand the space left for the engineers to integrate all the necessary components becomes smaller. When miniaturizing the RF front-end

module, the antenna is one of the most difficult components to reduce in size. This is mainly because the conventional resonant antenna size is highly dependent on the operational frequency, thus making the size reduction a challenging task. On the other hand there is a growing demand for faster data transfers, which in turn requires broadband and multi-band components. These two conflicting requirements must be met using low-cost solutions, that simultaneously maintain a high efficiency.

The emergence of a new class of materials called metamaterial (MTM) have attracted attention since their interesting electromagnetic characteristics have been proposed and experimentally verified. These properties are extensively applied to numerous applications in the microwave field including small antennas. The speciality of the zeroth order mode is the propagation constant in the structure is infinite and the size is independent of resonant frequency [25–29]. As a result the antenna dimensions in the resonant direction can be reduced. It has therefore been recognized by many researchers in the field that several important design constraints imposed by next-generation wireless systems can be addressed through the use of metamaterial technology.

1.5. Problem Statement

The proposed research consisted of numerical techniques and measurements to address the following question:

- Is it possible to design a passive UHF RFID antenna based on zeroth order resonance? If so, then what benefits in terms of miniaturization will it have over the traditional UHF RFID antenna design?

1.5.1. Technical Objectives

1. Develop the theory to design ZOR-based RFID antennas.

2. Choose an appropriate unit-cell that will allow study of the ZOR concept and the possibilities it presents towards RFID antenna design.

3. Validate the developed theory by designing a ZOR-based RFID antenna with commercially available software.

4. Explore the possibilities of miniaturizing the ZOR-based RFID antenna.

1.6. Objective of Thesis

In this thesis, novel compact antennas for passive UHF RFID tags are designed with CPW as host TL. Both interdigital capacitor (IDC) and shunt inductor based unit-cells have been studied. The IDC based antenna has been further studied for a more miniaturized design. All the simulated and measured results show good agreement. The final design is about $0.18\lambda_0 \times 0.14\lambda_0$ in size.

CHAPTER 2. RADIO FREQUENCY IDENTIFICATION (RFID)

A RFID system consists of an RFID reader which is a fairly complex and expensive transponder at one end and an RFID tag which is a simple and inexpensive device at the other end. RFID tags are handy in a way that they not only support a large number of distinct IDs as compared to the bar codes, but also they can incorporate additional information like manufacturer ID, product type or some other information of interest. However the biggest concern about their usage is their manufacturing cost. Although RFID tags are not as cheap as the traditional labeling bar code technologies, but offer enough added value services that they can be used for consumer retail goods.

RFID tags can be classified into three categories [1]:

- Active RFID tags: An active RFID tag is connected to either a power supply or use energy from an integrated battery. For the later case the tag's lifetime is limited and the tag works while the battery has enough energy to keep it running. Active RFID tags usually have long range of operation. An example of such a case could be transponders attached to airplane which identifies the national origin of plane.

- Semi-passive RFID tags: A semi-passive RFID tag has an integrated power supply attached to it, and it only starts working when electromagnetic power transmitted by the reader is incident on the tag. The integrated power supply can also be used for powering any auxiliary circuitry, for example a sensor which may be attached with the tag for a certain application. The additive feature of having an on-board integrated power supply enhances the maximum read range of the tag [1] as compared to the fully passive RFID tags because less power is required from the incoming incident field from the reader.

- Passive RFID tags: A passive RFID tag has no power source attached to it, and it harvests power for its operation from the incident electromagnetic field transmitted by the reader and has the lowest read range among the three.

The presence of power supply or integrated battery makes the active and semi-active RFID tags expensive, big in size and their lifetime is limited hence making them impractical for retail trade. However the passive RFID tags are cheap and have indefinite life time as they do not require a battery or maintenance which makes them a good choice for the retail trade.

RFID tags can also be classified from the operating frequency point of view into four categories [1]:

- Low frequency (LF) RFID tags which work at a frequency of 135 kHz.
- High frequency (HF) RFID tags which work at a frequency of 13.56 MHz.
- Ultra high frequency (UHF) RFID tags which work at 869 MHz in Europe, 915 MHz in North America and 956 MHz in Japan
- Microwave frequency RFID tags which work at 2.45 GHz or 5.8 GHz.

2.1. Passive RFID Operating Principle

Passive RFID tags are further divided into two classes: Near-Field RFID and Far-Field RFID.

2.1.1. Near-Field RFID

This type of tags work on Faraday's principle of magnetic induction. The RFID reader passes an alternating current through its coil which in result generates alternating magnetic field in vicinity. If there is a tag, which also has a small coil, lying in that vicinity, alternating voltage will be induced at tag's coil terminals which could be rectified and then used to power the tag's application specific integrated chip

(ASIC). On receiving sufficient power from the reader the ASIC changes the loading on tag's coil, in a predetermined fashion. This produces change in the flow of current at tag's coil thus generating its own magnetic field which will oppose the magnetic field of the reader and cause the change in flow of current at reader's coil. This change in current flow at the reader which is caused by change in magnetic field produced by the tag is the tag's ID. The principle is shown in Figure 2. Due to its simplicity of implementation this was the first approach that was developed for passive RFID tags. There are various standards defined for such a system such as ISO 15693 and ISO 14443 etc. However this approach has certain limitations such as the range for magnetic induction depends on $\frac{c}{2\pi f}$. Where c is velocity of light and f operating frequency. This shows increasing frequency will decrease range so near field RFID tags operate in LF/HF frequencies. Also the applications which have more ID bits or need discrimination between more than one tag in the same area require a high data rate from RFID tag meaning higher operating frequency which is a limiting factor for this case.

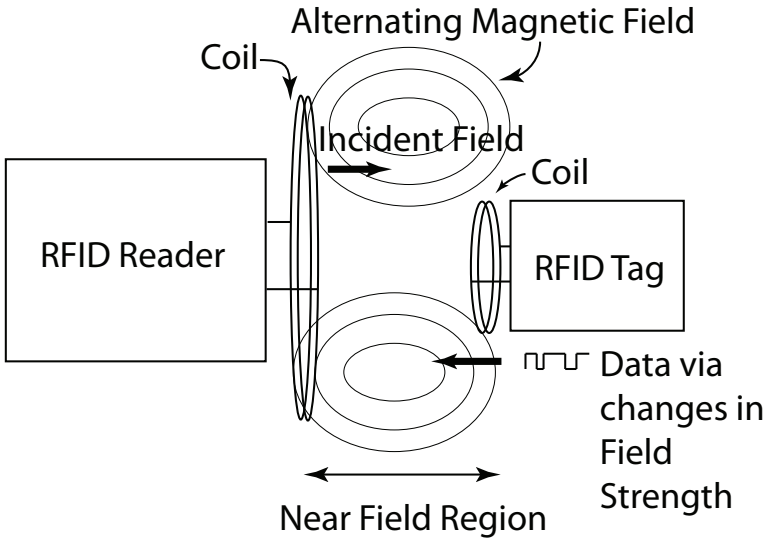

Figure 2. Near field RFID operation.

2.1.2. Far-Field RFID

Far-field RFID tags work using modulated backscatter. This type of tag, while lying in far-field and using a small dipole as an antenna, capture EM waves emitted by an RFID reader antenna, which usually is a dipole as well. These EM waves generate an alternating voltage at the terminals of tag's dipole which it can rectify and use to power its ASIC. The RFID tag antenna is tuned to a specific frequency such that for maximum power transfer its impedance at that frequency is equal to conjugate match of the ASIC impedance at that frequency. The RFID reader transmits the interrogating signal with timing information for the use of a passive RFID tag. As soon as a RFID tag comes within the maximum read range (also known as the interrogation zone [1]) of the RFID reader it receives the interrogating signal and feeds it to the RFID ASIC. The principle is shown in Figure 3. The RFID ASIC switches its impedance states between a lower and higher value in a predetermined and unique fashion (which represents its unique identity) as shown in Figure 4. The switching between impedance states changes the radar cross-section (RCS) of the tag antenna which as a result changes the backscattered power. This backscattered power is collected at the RFID reader and is used for identification and retrieval of stored information. Due to higher data rates and longer operating range demand for various applications, far-field RFID tags are getting more popular these days. There are various standards developed such as ISO 18000-6C or EPCglobal Gen 2, etc. Far-field RFID works on UHF/microwave frequencies. Their operating range is limited by the amount of energy that reaches the tag and by how sensitive the reader's receiver is to the reflected signal. The reflected signal strength is attenuated by $\frac{1}{d^4}$ where d is distance between the reader and the tag. However, the development in semiconductor field in recent times has significantly lowered the energy required to power a tag at a given frequency, thus increasing the operating range. Also, such radio receivers have

been developed which can detect a signal with power level of the order of -100 dBm at a reasonable cost.

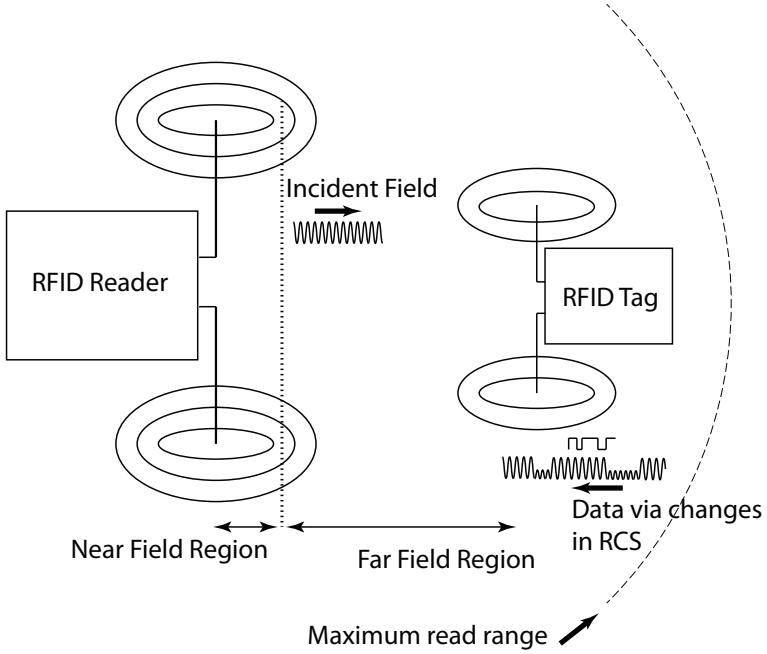

Figure 3. Far field RFID operation.

EPCglobal, a nonprofit organization initially setup by MIT Media Lab, played an important role in UHF RFID development. It has defined various standards, but its Class-1 Generation-1 96 bit RFID tag is receiving the most attention of late. This can label 10^{29} objects thus making it possible to uniquely label everything manufactured for the foreseeable future.

2.2. Impedance Matching of RFID Tag

Impedance matching between an RFID tag's antenna and an ASIC plays an important role in determining the performance of the tag such as: it determines the maximum range where a tag can communicate with the reader.

The antenna of the tag is directly connected to the ASIC as shown in the Thevenin equivalent circuit of the tag in Figure 4. $Z_a = R_a + jX_a$ is the complex antenna impedance and $Z_{c1,2} = R_{c1,2} + jX_{c1,2}$ are complex ASIC impedances in state

1 & 2. The ASIC impedance depends on frequency as well as input power. In order to have maximum power transfer from tag antenna to ASIC the antenna impedance is matched to the high impedance state of the ASIC. The frequency effect on impedance is determined by the ASIC's packaging and parasitic effect.

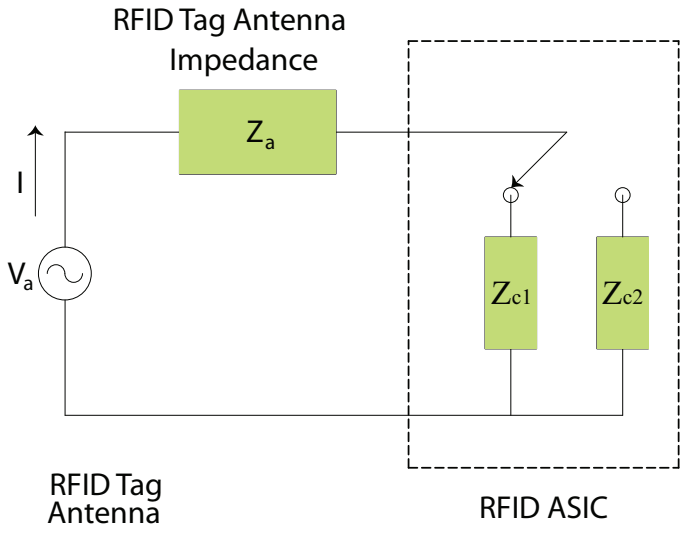

Figure 4. Thevenin equivalent circuit of RFID tag.

In order to have maximum range, the antenna impedance is matched to the ASIC's impedance at the minimum power required for ASIC to work. In most applications the tag continues to work if brought closer to the reader where the incident power will be greater. However, since the variation in ASIC impedance also depends on input power, it may occur that the increase in incident power has a severe effect on the impedance mismatch between the antenna and ASIC and even cause the tag not to respond within the operating zone.

2.3. Overview of RFID System

The functioning of an RFID system can be explained by the Friis transmission equation [30]:

$$P_r = P_t \frac{G_t G_r \lambda^2}{(4\pi R)^2} q \tag{2.1}$$

where P_r is the power received by RFID tag, P_t is the power transmitted by the RFID reader, G_r is the gain of tag antenna, G_t is the gain of reader, λ is the free-space wavelength of the operating frequency of reader, R is distance between reader and tag and q is impedance mismatch factor ($0 \leq$ q ≤ 1) between the impedance of the antenna on the tag and the input impedance of the ASIC on the tag. Equation (2.1) assumes a perfect polarization match between the antenna on the reader and the antenna on the RFID tag. Reorganizing (2.1) and solving for R, the following equation for determining the read range of a tag can be derived [31, 32] as:

$$R = \frac{\lambda}{4\pi}\sqrt{\frac{qG_tG_rP_t}{P_r}}. \tag{2.2}$$

If the minimum power required for tag operation is P_{th} then equation (2.2) can be written as:

$$R_{max} = \frac{\lambda}{4\pi}\sqrt{\frac{qG_tG_rP_t}{P_{th}}}. \tag{2.3}$$

Equation (2.3) is useful for designers to determine the maximum operating range of the tag. Typically the approach by a designer is to maximize R_{max}. One way of achieving this is to minimize the mismatch between the tag antenna and the ASIC input impedance or design a receiving antenna on the RFID tag with a maximized gain G_r. The other important factor in an RFID tag antenna design is the size of the antenna. Designers try to develop unique designs which offer smaller antennas while maintaining similar read ranges [8, 33–35]. Some common commercially available RFID tags and some unique miniaturized designs are shown in Figure 5.

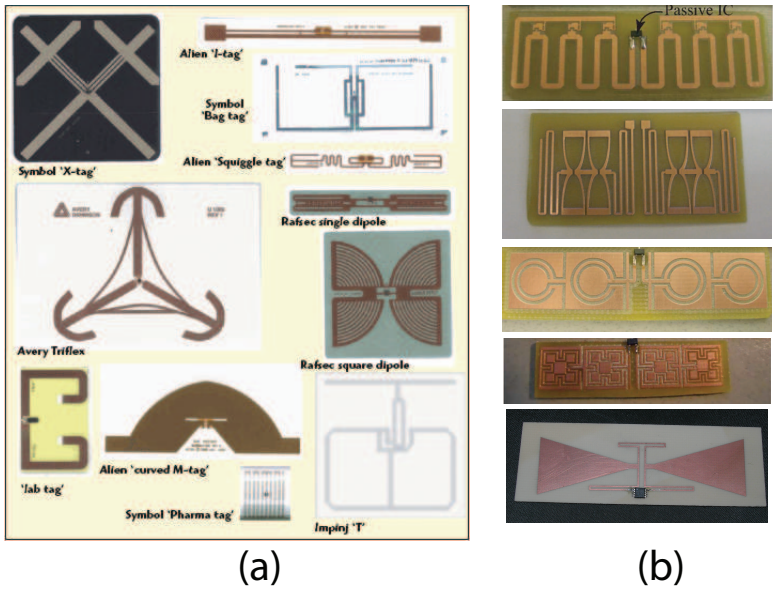

Figure 5. (a) Some commercially available RFID Tags and (b) Some unique RFID tags.

CHAPTER 3. CHARACTERIZATION OF CRLH-TRANSMISSION LINE AND APPLICATIONS

As explained in Section 1.2.1, metamaterial is an artificial structure. Metamaterials are usually formed by periodically repetitive structures. The fundamental structure is called a unit cell. The length of this unit cell in the direction of repetition is denoted as its period p. These unit cells are carefully designed so that their period is much smaller than the wavelength of the electromagnetic energy guided by that metamaterial. This behaves like a homogeneous medium to the guided electromagnetic energy. Different from conventional RH material, a metamaterial can exhibit a negative refractive index where the phase velocity is opposite to the group velocity thus making them anti-parallel [11]. In these materials the relative directions of the $(\vec{E},\ \vec{H},\ \vec{k})$ vector fields follow the left-hand rule; thus they are classified as "Left-Handed (LH)" materials. Here $\vec{E}$ is the electric field, $\vec{H}$ is the magnetic field, and $\vec{k}$ is the wave vector

In general conventional material, propagation of electromagnetic waves obeys the right-hand rule for the $(\vec{E},\ \vec{H},\ \vec{k})$ vector fields.The phase velocity direction is the same as the direction of the group velocity and the refractive index is a positive number. These materials are classified as "Right-Handed (RH)" materials. Most natural materials found in nature are RH materials. Artificial materials can also be RH materials.

3.1. Left-Handed Propagation in CRLH TL

The composite right/left hand (CRLH) transmission line (TL) exhibits a unique property of Zeroth Order Resonance (ZOR) [29,36]. At ZOR, the phase constant (β) becomes zero at a non-zero frequency indicating that the traveling wave has acquired an infinite wavelength. This unique property of CRLH-TL can be used to design compact and miniaturized antennas [25,37,38]. This means that at ZOR, physically

small antennas can be made to appear electrically large and hence the resonance will become independent of the antenna's physical dimensions. The resonance of such antennas will only depend on acquiring ZOR at a desired frequency by carefully adjusting their CRLH characteristics.

To help illustrate the use of ZOR properties to improve the gain and matching of a compact antenna on a passive UHF RFID tag, several properties of left-handed (LH) propagation are presented. It is well known that the equivalent circuit of a traditional printed microstrip TL consists of a series inductance and a shunt capacitance. The series inductance is caused by the current traveling down the printed TL and the shunt capacitance represents the capacitance between the printed signal conductors on one side of the board and the reference or ground plane. In fact, this inductance and capacitance exists on every printed TL (traditional or CRLH) because in the propagating band current is traveling down the TL and there is always capacitance between the conductors supporting this current and a reference conductor. When introducing the CRLH-TL, this series inductance and shunt capacitance is referred to as the parasitic values and are denoted in Figure 6 as L_R and C_R. The subscript R stands for right-handed (RH) propagation.

Next, to support LH-propagation, a series capacitance and a shunt inductance is introduced. These values are shown in Figure 6 and are denoted C_L and L_L, respectively. The subscript L stands for left-handed propagation. More particularly, the series capacitance is in series with the inductance and the shunt inductance is in parallel with the shunt capacitance. Therefore, to achieve LH-propagation, C_L and L_L should dominate over the values of L_R and C_R. Closer observation of the equivalent circuit in Figure 6 shows that the LH-values will only dominate over a certain band which is called the LH-propagating band. When the RH-values of L_R and C_R are dominant, this is called the RH-propagating band. When both the RH-

and LH-values are equal; this is called the transition frequency between the RH- and LH-propagating bands or simply the transition frequency. In practice, the series capacitance is usually introduced by placing interdigital capacitors (IDC) down the length of the TL [29]. The shunt inductance has been introduced in many different ways such as split ring resonators and shunt stubs [29].

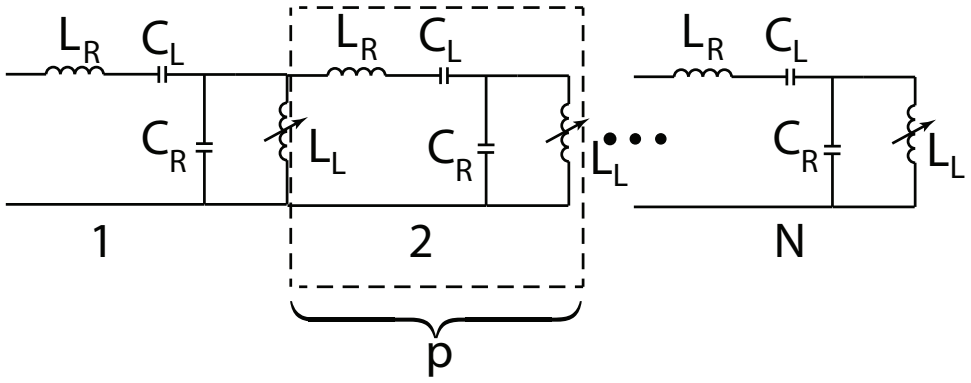

Figure 6. Reconfigurable CRLH-TL.

A CRLH-TL has several unique properties as a result of the introduction of C_L and L_L. The property used in this work is the sign change associated with the phase constant. The phase constant on a CRLH-TL is opposite to the phase constant on conventional RH-TL. This phase advance feature can be very useful for antenna designers and will be used in the next few sections to introduce the idea of ZOR antennas.

3.2. Lumped Microwave Components

Lumped components have the advantage of small size, low cost, and wide-band characteristics, but they do possess the disadvantage of having lower Q and lower power handling than distributed elements. To function well as a lumped element at microwave frequencies, the length of the lumped inductor and capacitor elements should not be longer than 12% of a wavelength λ, or they will begin to lose their lumped equivalence effect.

3.3. Distributed Microwave Components

Following sections discuss the realizations of microstrip inductors and capacitors which can be used to construct CRLH TL unit cells.

3.3.1. Microstrip Inductors

The inductance value of a microstrip TL inductor is determined from the total length, the number of turns, spacing, and line width. Narrow tracks are more inductive but they carry less current, so there is a trade-off between them. Spiral track inductors have more inductance because the magnetic fields from each turn of the spiral add up, creating a larger field through the middle of the spiral and mutual inductance between all the turns. The high-impedance, straight-line or wire inductor is the simplest form of an inductor, used for low inductance values (typically up to 3 nH), while the spiral inductor (circular or rectangular) can provide higher inductance values, typically up to 10 nH.

The meander-line inductor is used to reduce the area occupied by the element. In the meander inductor, adjacent conductors have equal and opposite current flow, which reduces the total inductance. Meander-line inductors have the advantage of lower eddy current resistance, but the disadvantage is lower inductance and lower self-resonant frequency than spiral inductors. Some commonly used inductor configurations are shown in Figure 7.

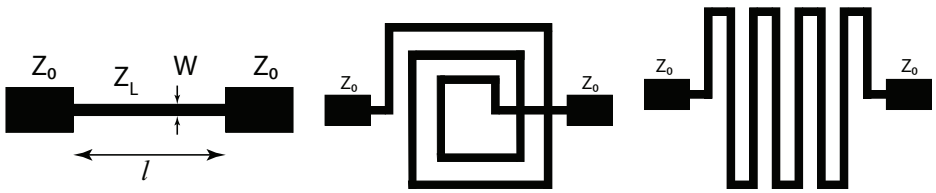

(a) Wire inductor (b) Square spiral (c) Meander line

Figure 7. Examples of microstrip inductors.

3.3.2. Microstrip Capacitors

Microstrip capacitors are formed due to discontinuities between closely placed conductors. The gap capacitor can be described as two coupled open-ended microstrip lines. The capacitance C in Figure 8 refers to the open-end capacitance, and the series gap capacitance C_g describes the electrical coupling. The interdigital capacitor relies on the strip-to-strip capacitance of parallel conducting fingers on a substrate, and it is suitable for applications where low values of capacitance are required. Some commonly used capacitor configurations are shown in Figure 8.

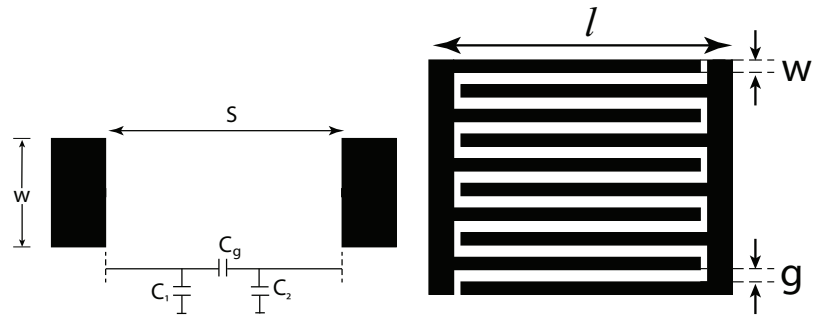

(a) Gap capacitor and equivalence circuit (b) Interdigital capacitor

Figure 8. Examples of microstrip capacitors.

3.4. Application of MTM TL

Metamaterial transmission lines have been applied to many fields successfully. They may extend the performance of conventional microwave components due to their unique dispersion characteristics. When the TL is used as a Zeroth Order Resonator (ZOR), it allows a constant amplitude and phase resonance across the entire resonator. Also, they may reduce the dimensions of some conventional microwave components greatly. The applications of MTM TL are

- Leaky-Wave Antennas
- Baluns

- Diplexers
- Directional couplers
- Power combiners/splitters

Furthermore, metamaterials can also be used on the ground plane interconnecting adjacent antennas in order to control the cross-talk of signals, thus reducing mutual coupling.

3.5. Current Work on ZOR Antennas

Recently there has been an immense focus by researchers on designing miniaturized ZOR antennas. In 2004, Sanada et al. [25] presented the four unit cell based ZOR antenna, shown in Figure 9(a), which resonated at 4.88 GHz. It was significantly smaller in dimensions as compared to the microstrip patch, shown in Figure 9(b), resonating at the same frequency. In 2005, Lim, Caloz and Itoh designed a scanning or beamwidth-controlling LW antenna. They showed that by controlling the voltage applied to each cell, the beam pattern of the antenna can be varied [39]. In 2007, Jae-Gon Lee and Jeong-Hae Lee proposed a novel low-profile omnidirectional antenna using zeroth-order resonance of mushroom structure. The mushroom structure provides uniform vertical electric field which in give rise to a structurally stable low-profile omnidirectional radiation pattern [40]. Lai, Leong and Itoh proposed different configurations of ZOR antennas with monopolar radiation patterns. They showed that a higher number of cells can be used to increase the peak gain with minimal effect on the resonant frequency. Thus the antenna size/gain can be controlled independently of the antennas frequency [41]. Later in 2007 Park et al. [27] proposed the miniaturized epsilon negative (ENG) and double negative (DNG) ZOR antennas shown in Figure 10. They also showed that an increased number of unit cells can be used to increase the peak gain.

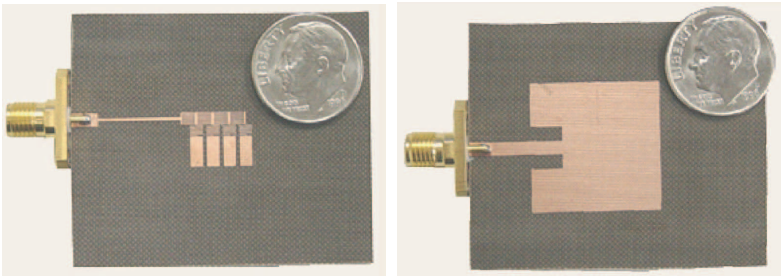

(a) (b)

Figure 9. (a) Four-cell ZOR antenna (f_0 = 4.88 GHz) and (b) Microstrip patch antenna on the same substrate (f_0 = 4.90 GHz).

(a) (b)

Figure 10. (a) Three-cell DNG ZOR antenna and (b) Three-cell ENG ZOR antenna.

In 2009, Ji, Kim and Seong proposed a compact multiband antenna based on DNG ZOR for a wireless mobile system [42]. The authors reported that their proposed antenna has good radiation characteristics and is more compact as compared to various multiband planar inverted-F antennas used for mobile systems. Pyo et al. proposed in [43] a slot loaded CRLH-TL metamaterial structure using rectangular and hexagonal unit cells. The authors showed that the presence of the slot can improve the radiation efficiency by reducing the Q factor of the shunt resonance.

Later in 2009, Kim et al. proposed a ZOR based tunable internal antenna for DVB-H service. To achieve the wide bandwidth required for DVB-H service,

a variable capacitor was added between the transmission line and the ground. In addition, the antenna gain was improved by using helical radiators [44]. In 2010, Ji, Kim and Seong proposed a method to extend the bandwidth of metamaterial antennas using CRLH-TL. The authors showed that by using a smaller value of loaded series capacitance on the CRLH-TL, the bandwidth can be extended by merging the zeroth-order and the first-negative-order resonance frequencies together in a single passband [45]. Sipal, Ajami and Heberling studied the effects of substrate dimensions on ZOR antennas. The authors found that reduced substrate size results in a wider bandwidth but lower realized gain. They also proposed that metallic walls employed on the edges will effectively increase the size of the ground plane. Thus doing so will make the bandwidth independent of the substrate dimensions, while the gain deterioration will be significantly alleviated as well [46]. In 2011, Park and Lee proposed an omnidirectional circularly polarized ZOR antenna using a circular mushroom structure with the curved branches. The antenna uses the ZOR mode of ENG TL to obtain the omnidirectional radiation pattern and vertical polarization. Also, horizontal polarization is achieved by the curved branches [28]. Lai et al. proposed ZOR antennas based on capacitor-loaded and inductor loaded unit cells. The authors also discussed and introduced the condition for ZOR for the case of a lossy structure [47]. In 2013, Chiu, Lai and Chen [48] proposed a dual-band ZOR antenna with series and shunt resonances. The authors proposed a series of simple termination circuits, including two pseudo-open and two pseudo-short designs. These proposed terminations are based on the observations of the termination effects on the zeroth- order series and shunt resonances. These terminations enable simultaneous excitation of the zeroth-order resonances for unbalanced CRLH-TLs, as shown in Figure 11.

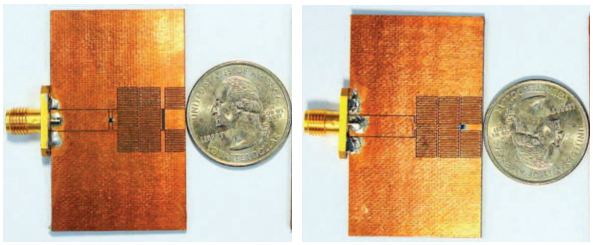

(a) (b)

Figure 11. (a) Two-cell ZOR antenna with $f_{se} < f_{sh}$ and (b) Two-cell ZOR antenna with $f_{sh} < f_{se}$.

In this section it can be seen that significant research is still being conducted on ZOR antennas. But throughout this summary it is also obvious that ZOR based UHF RFID antennas had not been studied prior to this present work.

CHAPTER 4. COPLANAR-WAVEGUIDE STRUCTURES

The term "coplanar" means sharing the same plane. This is the type of transmission line where the reference conductors are in the same plane as that of the signal carrying-conductor. The signal-carrying conductor is placed in the middle with a reference plane conductor on both sides, as shown in Figure 12. The advantage of having both conductors in the same plane lies in the fact that it is easier to mount lumped components between the two planes and it is easier to realize shunt and series configurations. The CPW was first proposed by Wen [49] and, since then, has been used extensively in wireless communications [50, 51].

The disadvantage of a CPW is that it can be difficult to maintain the same potential between the reference and signal conductors throughout the signal trace. Nevertheless, many advances have been made using CPW transmission lines such as novel filters [52] and right/left handed propagation [53].

Several properties of the CPW-TL in Figure 12 are derived next. These expressions will be useful to explain the ZOR phenomenon later. The attenuation and phase constants can be derived by performing a quasi-static analysis of a CPW [54]. The phase velocity and characteristic impedance equations can be written as [54]:

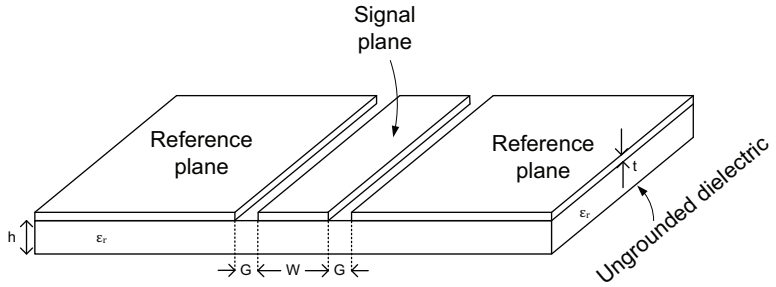

Figure 12. CPW transmission line on ungrounded dielectric.

$$v_p = \sqrt{\frac{2}{\epsilon_r + 1}}c \tag{4.1}$$

and

$$Z_0 = \frac{30\pi}{\sqrt{\epsilon_{re}^t}} \frac{K(k_e^{'})}{K(k_e)}. \tag{4.2}$$

where

$$k_e \cong k + \frac{(1-k^2)\Delta}{2G}, \tag{4.3}$$

$$k = \frac{W}{W + 2G}, \tag{4.4}$$

$$\Delta = \frac{1.25t}{\pi}\left(1 + \ln\frac{4\pi W}{t}\right), \tag{4.5}$$

$$k^{'} = \sqrt{1-k^2}, \tag{4.6}$$

$$\epsilon_{re}^t = \epsilon_{re} - \frac{0.7(\epsilon_{re}-1)t/G}{\frac{K(k_e)}{K(k_e^{'})} + \frac{0.7t}{G}} \tag{4.7}$$

and

$$\begin{aligned}\epsilon_{re} =& \frac{\epsilon_r + 1}{2}\Bigg\{\tanh(1.785\log(h/G) + 1.75) + \\ & \frac{kG}{h}\Big(0.04 - 0.7k + 0.01(1 - 0.1\epsilon_r)(0.25 + k)\Big)\Bigg\}.\end{aligned} \tag{4.8}$$

Here W is the width of the center conductor, G is the spacing between the center conductor and the reference conductor, ϵ_r is the relative permittivity of the dielectric, c is the speed of light and t is the thickness of the conductor. $K(k)$ is the complete elliptic integral of the first kind and the ratio $K(k)/K(k^{'})$ has been reported in [54, 55] as:

$$\frac{K(k_e^{'})}{K(k_e)} = \begin{cases} \frac{\pi}{\ln\left(2\frac{1+\sqrt{k}}{1-\sqrt{k}}\right)} & 0 \le k \le 0.707 \\ \frac{1}{\pi}\ln\left(2\frac{1+\sqrt{k}}{1-\sqrt{k}}\right) & 0.707 \le k \le 1. \end{cases} \tag{4.9}$$

Using equations (4.1) - (4.9) the attenuation constant due to ohmic losses can be calculated as [54]:

$$\alpha_c = 4.88 \times 10^{-4} R_s \epsilon_{re} Z_0 \frac{P'}{\pi G} \left(1 + \frac{W}{G}\right) \left(\frac{\frac{1.25}{\pi} \ln \frac{4\pi W}{t} + 1 + \frac{1.25t}{\pi W}}{\left(2 + \frac{W}{G} - \frac{1.25t}{\pi G}\left(1 + \ln \frac{4\pi W}{t}\right)\right)^2} \right). \quad (4.10)$$

where

$$P' = \left(\frac{K(k_e)}{K(k_e')}\right)^2 P, \quad (4.11)$$

$$P = \begin{cases} \frac{k}{(1-\sqrt{1-k^2})(1-k^2)^{3/4}} & 0 \le k \le 0.707 \\ \frac{1}{(1-k)\sqrt{k}} \left(\frac{K(k_e)}{K(k_e')}\right)^2 & 0.707 \le k \le 1 \end{cases} \quad (4.12)$$

and

$$R_s = \sqrt{\rho \pi f \mu}. \quad (4.13)$$

The attenuation constant due to dielectric losses is [54]:

$$\alpha_d = 27.3 \frac{\epsilon_r}{\sqrt{\epsilon_{re}}} \frac{\epsilon_{re} - 1}{\epsilon_{re} + 1} \frac{\tan \delta}{\lambda_0} \quad \text{dB/unit length.} \quad (4.14)$$

here $\tan \delta$ is the loss tangent of the dielectric, and the total attenuation of the CPW structure can be written as:

$$\alpha_{cpw} = \alpha_c + \alpha_d. \quad (4.15)$$

The phase constant of the CPW structure can be calculated as [50]:

$$\beta_{cpw} = \frac{2\pi f}{v_c}. \quad (4.16)$$

Next, these expressions will be used to introduce the interdigital capacitor loaded CPW which will then be used to explain ZOR.

4.1. Interdigital Capacitor Loaded CPW

An Interdigital capacitor loaded transmission line provides a series resonance. The Zeroth Order Resonance (ZOR) of an interdigital capacitor (IDC) loaded CPW has been investigated and reported in [47]. The equivalent transmission line model of an interdigital capacitor loaded transmission line is shown in Figure 13 and consists of two symmetric transmission lines interconnected with a series capacitance. The host transmission line has been shown equally divided into two parts. Since the size of the unit cell is much smaller than the guided wavelength, the transmission line can be modeled with an equivalent circuit with a series inductance and shunt capacitance.

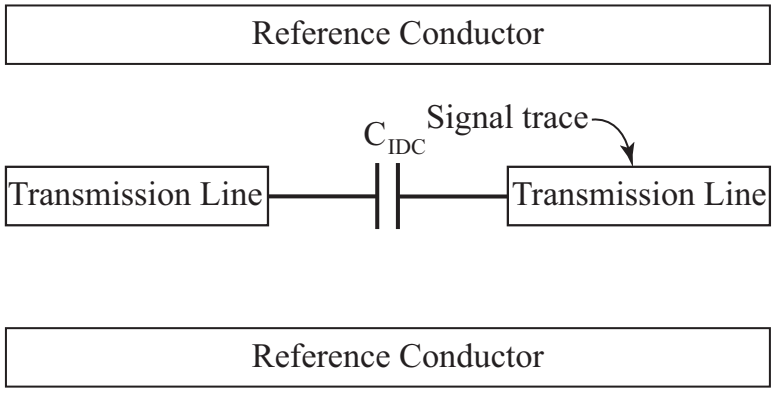

Figure 13. Equivalent circuit model of interdigital capacitor loaded CPW.

The layout of the interdigital capacitor based unit cell is shown in Figure 14. The capacitance between the interdigital capacitor and bilateral ground plane is fairly small as compared to the series capacitance of the interdigital capacitor, so it can be neglected. This unit cell can be repeated periodically to design the ZOR antenna.

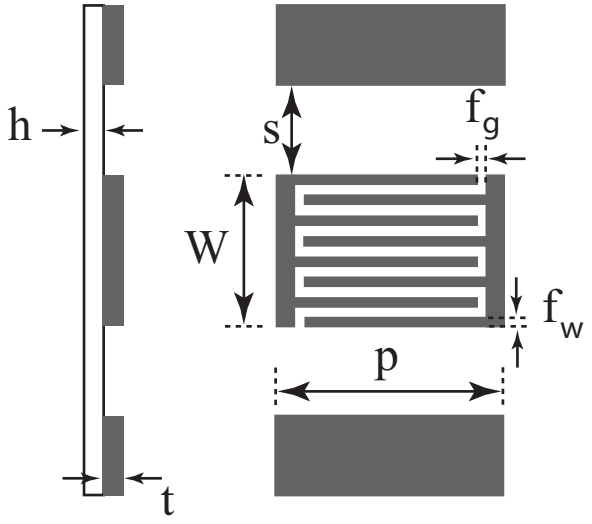

Figure 14. Interdigital capacitor loaded CPW unit cell.

Since the unit cell will be repeated periodically and will be symmetric about the port of the antenna, it will resemble the TL in Figure 13. Therefore, the propagation constant γ (where $\gamma = \alpha + j\beta$) and characteristic impedance (also known as the Bloch impedance) Z_B can be expressed in terms of an ABCD matrix as [50]:

$$A = \cosh \gamma L \tag{4.17}$$

and

$$Z_B = \frac{BZ_0}{\sqrt{A^2 - 1}}. \tag{4.18}$$

Here L is the length of the unit cell, and Z_0 is the characteristic impedance of the CPW. Note that equations (4.17) and (4.18) are derived based on the assumption that the unit cells are symmetric, and hence A = D. The propagation constant of the TL is $\gamma_{cpw} = \alpha_{cpw} + \beta_{cpw}$ where α_{cpw} and β_{cpw} can be calculated from equations (4.15) and (4.16), respectively.

Next, the ABCD matrix of the circuit shown in Figure 13 can be determined as [50]:

$$\begin{bmatrix} A & B \\ C & D \end{bmatrix}_{cpw} = \begin{bmatrix} \cosh\frac{\gamma_{cpw}L}{2} & Z_0 \sinh\frac{\gamma_{cpw}L}{2} \\ Y_0 \sinh\frac{\gamma_{cpw}L}{2} & \cosh\frac{\gamma_{cpw}L}{2} \end{bmatrix} \tag{4.19}$$

and

$$\begin{bmatrix} A & B \\ C & D \end{bmatrix}_{IDC} = \begin{bmatrix} 1 & \frac{1}{j\omega C_L} \\ 0 & 1 \end{bmatrix}. \tag{4.20}$$

Here, $L/2$ represents half of the CPW length. The ABCD matrix of the whole unit cell shown in Figure 13 can be calculated from equations (4.19) and (4.20) as:

$$\begin{bmatrix} A & B \\ C & D \end{bmatrix} = \begin{bmatrix} A & B \\ C & D \end{bmatrix}_{cpw} \times \begin{bmatrix} A & B \\ C & D \end{bmatrix}_{IDC} \times \begin{bmatrix} A & B \\ C & D \end{bmatrix}_{cpw}. \tag{4.21}$$

From equation (4.21), parameter A can be calculated and equation (4.17) can be written as:

$$\cosh\alpha L \cos\beta L + j \sinh\alpha L \sin\beta L = X + \frac{Y}{j2\pi Z_0 \omega C_L}. \tag{4.22}$$

where

$$X = \cosh\alpha_{cpw} L \cos\beta_{cpw} L + j \sinh\alpha_{cpw} L \sin\beta_{cpw} L \tag{4.23}$$

and

$$Y = \sinh\alpha_{cpw} L \cos\beta_{cpw} L + j \cosh\alpha_{cpw} L \sin\beta_{cpw} L. \tag{4.24}$$

In equation (4.22) α represents the attenuation constant and β represents the phase constant of the Bloch wave propagating on the unit cell whereas α_{cpw} and β_{cpw} are attenuation and phase constants, respectively, of the host CPW-TL.

For comparison, equation (4.22) can be separated into real and imaginary parts which gives:

$$\frac{\cosh \alpha L \cos \beta L}{\cosh \alpha_{cpw} L} = \cos \beta_{cpw} L + \frac{\sin \beta_{cpw} L}{j2\pi Z_0 \omega C_L} \tag{4.25}$$

and

$$\frac{\sinh \alpha L \sin \beta L}{\sinh \alpha_{cpw} L} = \sin \beta_{cpw} L - \frac{\cos \beta_{cpw} L}{j2\pi Z_0 \omega C_L}. \tag{4.26}$$

The unknowns in equations (4.25) and (4.26) are α and β of the Bloch wave. Solving for α and β gives:

$$\alpha = \frac{1}{L} \cosh^{-1} \left(\frac{F_+}{2} \right) \tag{4.27}$$

and

$$\beta = \frac{1}{L} \cosh^{-1} \left(\frac{F_-}{2} \right). \tag{4.28}$$

where $F_\pm = \sqrt{S^2 + (R+1)^2} \pm \sqrt{S^2 + (R-1)^2}$, and R and S are right-hand sides of (4.25) and (4.26) times the denominator on their corresponding left-hand side respectively. The key idea when designing a ZOR antenna is to determine the frequency at which equation (4.28) is equal to zero. Since the propagation constant is inversely proportional to the wavelength, when equation (4.28) is zero, the wavelength at that frequency is equal to infinity. At this frequency, the antenna looks infinitely long electrically, and hence it can be claimed that the dimensions of the antenna have been made independent of the operating wavelength.

4.2. ZOR Analysis of Interdigital Capacitor Loaded CPW

In this section, the dispersion characteristics of an interdigital capacitor loaded CPW will be investigated by using the above formulas, and the condition of the zeroth-order resonance will be discussed.

Consider the unit cell depicted in Figure 14, and assume the host CPW to be lossless. In this case, the unit cell is designed on a lossless substrate, Rogers TMM4 ($\epsilon = 4.5$), but with a vanishing loss tangent ($\tan\delta = 0$) and with its metallic cladding made of a perfect electrical conductor. For demonstration, the design parameters of the unit cell in Figure 14 are chosen as $W = 8.82$ mm, $S = 7.96$ mm, $L = 17.56$ mm, $H = 1.524$ mm, and $C_L = 2.75$ pF. The dispersion relation of this unit cell can be calculated with (4.27) and (4.28), and the results obtained are plotted in Figure 15. One can observe that as the frequency is increased up to 885 MHz, the attenuation constant α decreases monotonically to zero while the phase constant β remains zero. Beyond 885 MHz, α is constantly zero while β increases monotonically.

For the lossless case, the threshold frequency, at which $\alpha = \beta = 0$, is known as the zeroth-order resonant frequency. The most interesting feature of this resonance is the so-called infinite wavelength property, which in theory could produce a uniform field distribution along the entire structure. As a result, the zeroth-order resonant frequency is independent of its physical dimensions. The zeroth-order resonance of an interdigital capacitor loaded CPW is in the form of series resonance. Thus the associated resonant frequency can be denoted as ω_{se}.

In practice, the losses within the host CPW must be considered. By setting $\tan\delta = 0.002$ for the Rogers TMM4 substrate and $\sigma = 5.8 \times 10^7$ S/m for the copper cladding in the above design, the dispersion relations for the lossy unit cell can also be obtained through equations (4.27) and (4.28), and they are plotted in Figure 15. One can see that the responses resemble those of the lossless case except for the nonzero phase constant at frequencies below 885 MHz and nonzero attenuation constant beyond that. Therefore, the condition of the zeroth-order resonant frequency is amended as the frequency at which $\alpha = \beta$ for general applicability. With equations (4.27), (4.28), and this modified resonant condition, the explicit formula

for calculating the C_L needed to sustain a specified resonant frequency can also be derived. For the lossy interdigital capacitor loaded CPW, the relation between the series capacitance (C_L) and the resonant frequency ω_{se} is derived as:

$$C_L = \frac{\cosh \alpha_{cpw} L \sin \beta_{cpw} L}{2\omega_{se} Z_0 (1 - \cosh \alpha_{cpw} L \cos \beta_{cpw} L)}. \tag{4.29}$$

For a given zeroth-order resonant frequency, one may use (4.29) to predict the value of the series capacitance C_L. Note that by setting $\alpha_{cpw} L = 0$, (4.29) reduces it to its lossless counterpart. Moreover, for C_L to be positive-valued, we have:

$$\cosh \alpha_{cpw} L \sin \beta_{cpw} L (1 - \cosh \alpha_{cpw} L \cos \beta_{cpw} L) > 0. \tag{4.30}$$

This indicates that the length of a unit cell L should be shorter than about half a guided wavelength. This is always satisfied because the length of a unit cell is recommended to be shorter than a quarter of a guided wavelength [56], [57].

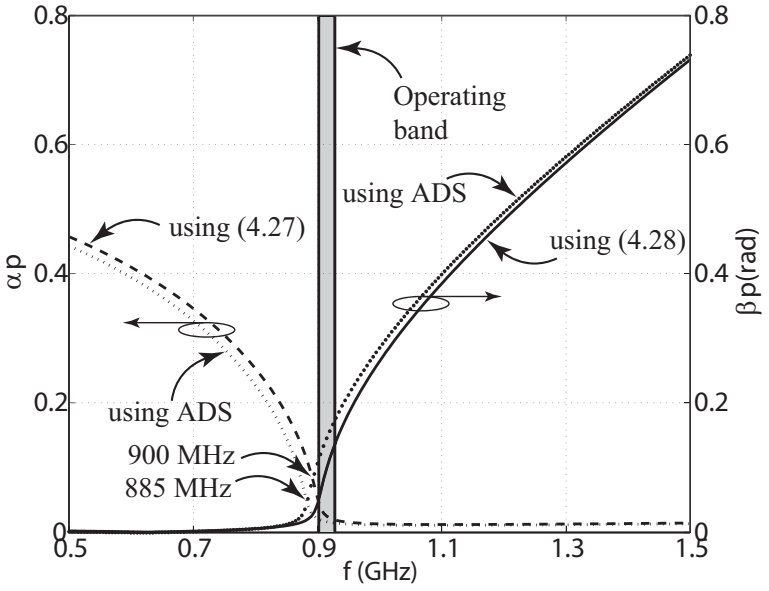

Figure 15. Dispersion diagrams of lossless and lossy capacitor loaded CPW.

CHAPTER 5. ZOR RFID ANTENNA DESIGN

5.1. Design of the IDC Unit-Cell

In this section, the method of using the dispersion characteristics to design the IDC unit-cell in Figure 14 for an antenna on a passive UHF RFID tag is presented. The first step is to determine the capacitance required to obtain ZOR at the desired frequency (i.e., the frequency where $\alpha = \beta$). For this work, the operating frequency has been selected as 920 MHz which is the RFID operating frequency in North America. Therefore, to introduce inductance the ZOR frequency of the IDC unit-cell is defined to be 900 MHz. Choosing the ZOR frequency depends on the application. If the main purpose is to reduce the overall size of the antenna, then more inductance may be desirable and a lower ZOR frequency can be chosen. For this work, the antenna is required to be a conjugate match at the operating frequency of 920 MHz to a passive RFID IC attached to the port of the antenna. This then requires the resonant frequency of the antenna and ZOR frequency of the IDC unti-cell to be approximately 900 MHz [10].

Next, using (4.25) and (4.25), the required capacitance for a desired ZOR frequency can be calculated as [47]:

$$C_{IDC} = \frac{\cosh \alpha_{CPW} p \sin \beta_{CPW} p}{2\omega_r Z_0 (1 - \cosh \alpha_{CPW} p \cos \beta_{CPW} p)}. \tag{5.1}$$

where $\omega_r = 2\pi(9)(10^8)$Hz. Equation (5.1) has several uses. Overall, (5.1) can be used in an iterative manner (in software) to determine the dimensions of an IDC unit-cell which can not only be manufactured practically but will also exhibit the required impedance characteristics. More specifically, the gap between the fingers and the length of the fingers can be computed and checked for manufacturability. Furthermore, the values of W and s are a result of these computations. These values

define the overall layout size of the antenna. If the values of the finger gap, the finger length, W or s are not desirable, further iterations can be conducted.

After several design iterations using equation (5.1), the final dimensions of the IDC unit-cell in Figure 14 were determined to be $W = 8.82$ mm, finger width $f_w = 0.66$ mm, finger gap $f_g = 0.36$ mm, $p = 17.56$ mm, $s = 7.96$ mm, substrate thickness $h = 1.524$ mm and conductor thickness $t = 35\mu$m. Rogers TMM4 ($\epsilon_r = 4.5$ and $\tan\delta = 0.002$) was used as a substrate and the conductivity of the conductors was $\sigma = 5.8 \times 10^7$. From equation (5.1) the computed capacitance to obtain ZOR at 900 MHz was found to be $C_{IDC} = 2.64$ pF. The dispersion characteristics of the IDC unit-cell are computed using equations (4.27) and (4.28) and are plotted in Figure 16. The curves that cross at 900 MHz are the dispersion characteristics of the ICD unit-cell computed using equation (5.1). It is shown that the phase constant (β) is non-zero below the ZOR frequency and similarly the attenuation constant (α) is non-zero after the ZOR frequency. Here the ZOR frequency is taken as the point at which $\alpha = \beta$ and it is below the operating band.

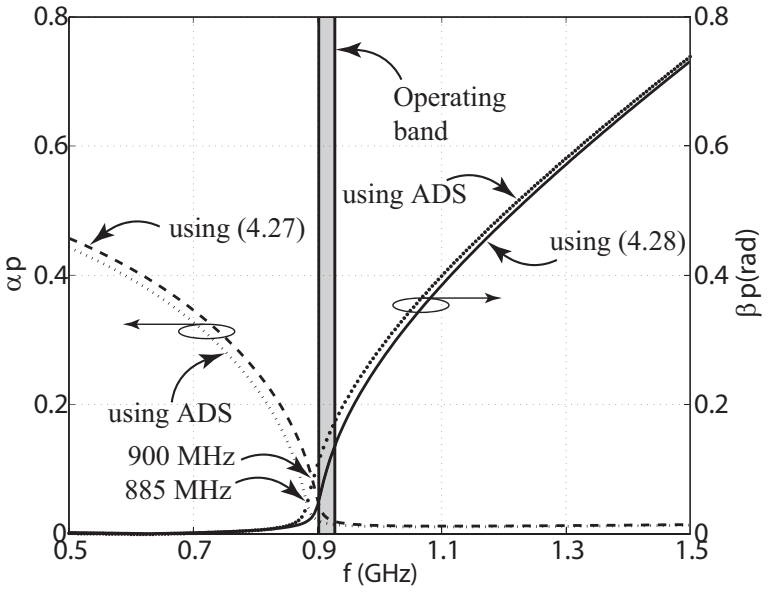

Figure 16. Dispersion characteristics of the IDC Unit-cell.

5.2. Prototype Antenna Design I

The proposed antenna shown in Figure 17 consists of four series connected IDC unit-cells. The proposed antenna has an open circuit at one end and a short circuit line on the other end. The final dimensions were determined in HFSS [58] to have a conjugate match at 920 MHz with the passive Higgs-2 [59] RFID IC attached to the port. As with the IDC unit-cell, the antenna was simulated in HFSS on a Rogers TMM4 substrate with $\epsilon_r = 4.5$, $\tan\delta = 0.002$ and a substrate thickness $h = 1.524$ mm. The manufactured prototype tag and the simulated input impedance is shown in Figure 20. Note that the input impedance ($Z_{in} = 15 + j145\Omega$) of the antenna is close to conjugate value of the input impedance of the Higgs-2 IC ($Z_{IC} = 13.73 - j142.8\Omega$) at 920 MHz.

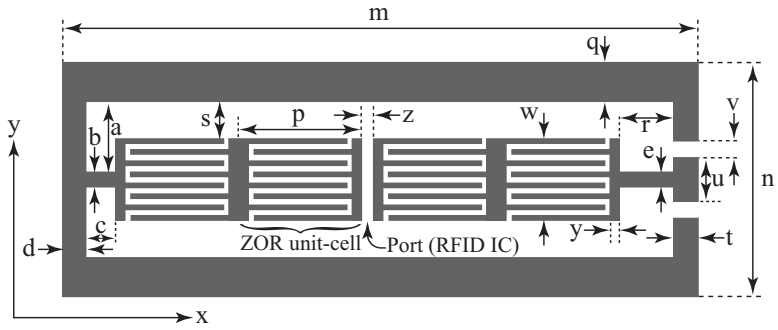

Figure 17. Layout of the ZOR antenna for a passive UHF RFID tag design I with a = 12.16 mm, b = 0.4 mm, c = 5.0 mm, d = 1.0 mm, e = 0.4 mm, m = 83.2 mm, n = 38.4 mm, w = 8.82 mm, p = 17.56 mm, s = 7.96 mm, q = 6.8 mm, r = 5.0 mm, t = 1.0 mm, u = 3.0 mm, v = 0.35 mm, y = 1.0 mm and z = 1.0 mm.

Next, for comparison, the equivalent circuit of the RFID antenna shown in Figure 18 was extracted using the software tool Advanced Design System (ADS) [60] and compared to HFSS simulations. The extracted values are shown in the caption of Figure 18, and the IDC capacitance was found to be $C_{extracted} = 2.75$ pF. The dispersion characteristics of the IDC unit-cell were also computed using

equations (4.27) and (4.28) with the extracted capacitance. These results are plotted in Figure 19 for the lossy case. The curves that cross at 885 MHz are the dispersion characteristics of the ICD unit-cell computed using the circuit extraction method. It is shown that the ZOR frequency (i.e., where $\alpha = \beta$) is $f_{ZOR} = 885$ MHz, which is below the operating band of the passive RFID tag. Furthermore, the input impedance of the prototype antenna was computing using the equivalent circuit. These results are shown to agree with HFSS in Figure 20 and Figure 21. The physical dimensions of the antenna are found to be $0.26\lambda_0 \times 0.12\lambda_0$.

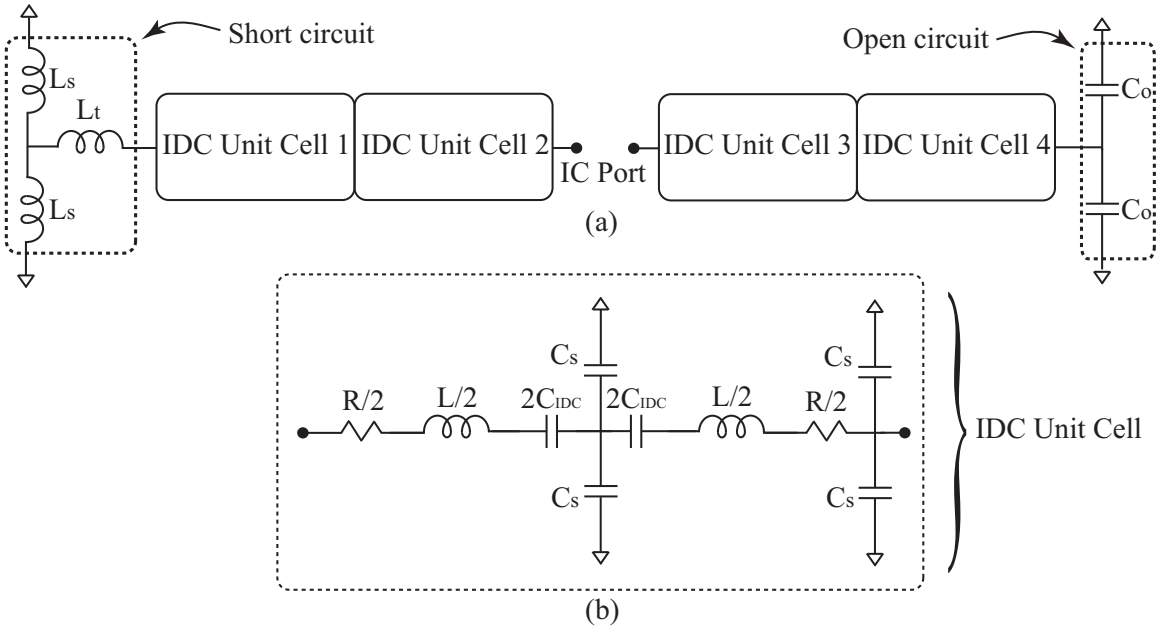

Figure 18. (a) Equivalent circuit of the proposed ZOR RFID antenna design I and (b) Equivalent circuit of an individual IDC unit-cell ($R = 1.3\ \Omega$, L = 6.75 nH, $C_{IDC} = 2.75$ pF, C_s = 0.18 pF, $L_s = 13.0$ nH, $L_t = 4.51$ nH and $C_o = 0.18$ pF).

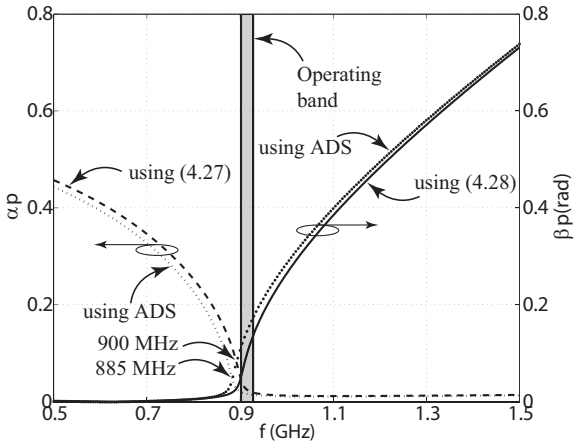

Figure 19. Dispersion diagrams of the lossy CPW IDC Unit-cell.

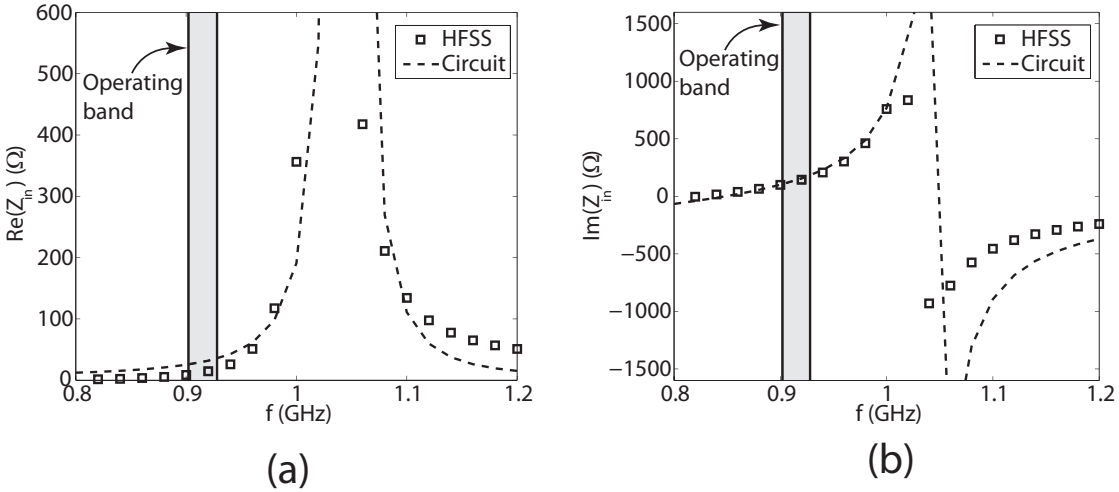

Figure 20. (a) Input resistance of the prototype antenna design I and (b) input reactance of the prototype antenna design I.

Next, to measure the read-range of the prototype RFID tag, an Alien Technologies ALR-9900 RFID reader having maximum output power of 1 W was used [59]. The RFID reader was connected to a circularly polarized antenna with a gain of 6 dBi and the prototype RFID tag was placed in an anechoic chamber with the reader antenna. An image of the prototype tag being measured in the anechoic chamber is shown in Figure 22.

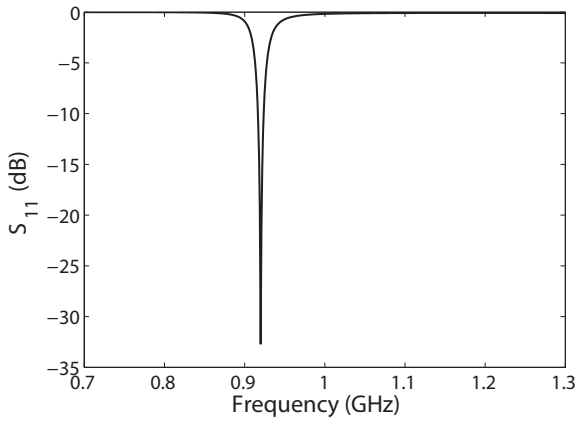

Figure 21. S_{11} of the prototype antenna design I.

Figure 22. Prototype antenna design I being measured in the anechoic chamber.

Because of the limited size of the chamber, a maximum read-range could not be determined by moving the tag away from the reader until it could no longer be read. An alternate method has been provided in [61] for such cases where it is not possible to directly measure the maximum read-range due to space limitations. Using the method outlined in [61], the maximum achievable read-range can be predicted based on system power levels and measurements for a known distance between the antenna on a RFID reader and the tag under test. This method uses the Friis transmission equation and the fact that a certain minimum power is required to activate the RFID

tag. Using this information the output power of the RFID reader was reduced until the reader initially detected the prototype tag at a distance of 3.4 m. This value is denoted as $R_{measured}$. The required attenuation to initiate the reading of the tag is denoted as α_{dB} and was determined to be 7 dB. Then the following equation was used to predict the maximum read-range: $R_{max} = 10^{\alpha_{dB}/20} R_{measured}$. This then resulted in $R_{max} = 7.6$ m.

5.3. Prototype Antenna Design II

The next step is to reduce the size of the antenna as developed in section 5.2. For this, if we carefully study equation (5.1), we can see that by reducing the period p while keeping everything else essentially the same the denominator is decreased resulting in a higher value of the required C_{IDC}. This indicates that if the dimension is to be reduced by reducing unit-cell size, the capacitance it produces should be increased. Following this approach, a similar procedure was followed as in section 5.2, and the dimensions, $W = 15.2$ mm, finger width $f_w = 2.2$ mm, finger gap $f_g = 0.4$ mm, $p = 12$ mm, $s = 9$ mm for new unit-cell were derived. The proposed antenna shown in Figure 23 consists of four series connected IDC unit-cells. The proposed antenna has a short circuit at both ends.

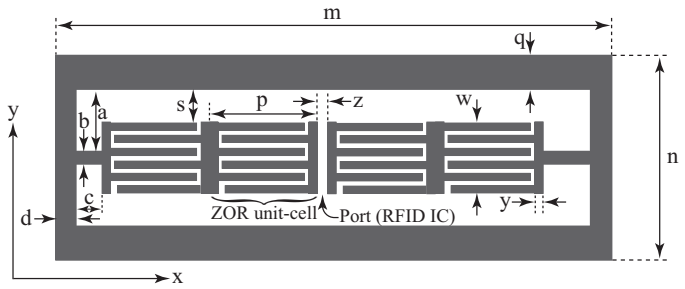

Figure 23. Layout of the ZOR antenna for a passive UHF RFID tag design II with a = 16.3 mm, b = 0.6 mm, c = 3.5 mm, d = 1.0 mm, e = 0.6 mm, m = 58 mm, n = 44.8 mm, w = 15.2 mm, p = 12 mm, s = 9 mm, q = 5.8 mm, r = 3.5 mm, t = 1.0 mm, y = 1.0 mm and z = 1.0 mm.

The equivalent circuit of the RFID antenna shown in Figure 24 was extracted in ADS, and was compared to HFSS simulations. The extracted values are shown in the caption of Figure 24, and the IDC capacitance was found to be $C_{extracted} = 4.1$ pF. The dispersion characteristics of the IDC unit-cell were also computed using equations (4.27) and (4.28) with the extracted capacitance. These results are plotted in Figure 25 for the lossy case. The curves that cross at 923 MHz are the dispersion characteristics of the ICD unit-cell computed using the circuit extraction method. It is shown that the ZOR frequency (i.e., where $\alpha = \beta$) is $f_{ZOR} = 923$ MHz. Furthermore, the input impedance of the prototype antenna was computed using the equivalent circuit. These results are shown to agree with HFSS in Figure 26 and Figure 27. The physical dimensions of the antenna are found to be $0.18\lambda_0 \times 0.13\lambda_0$. This means that an over all size reduction of about 19% is achieved.

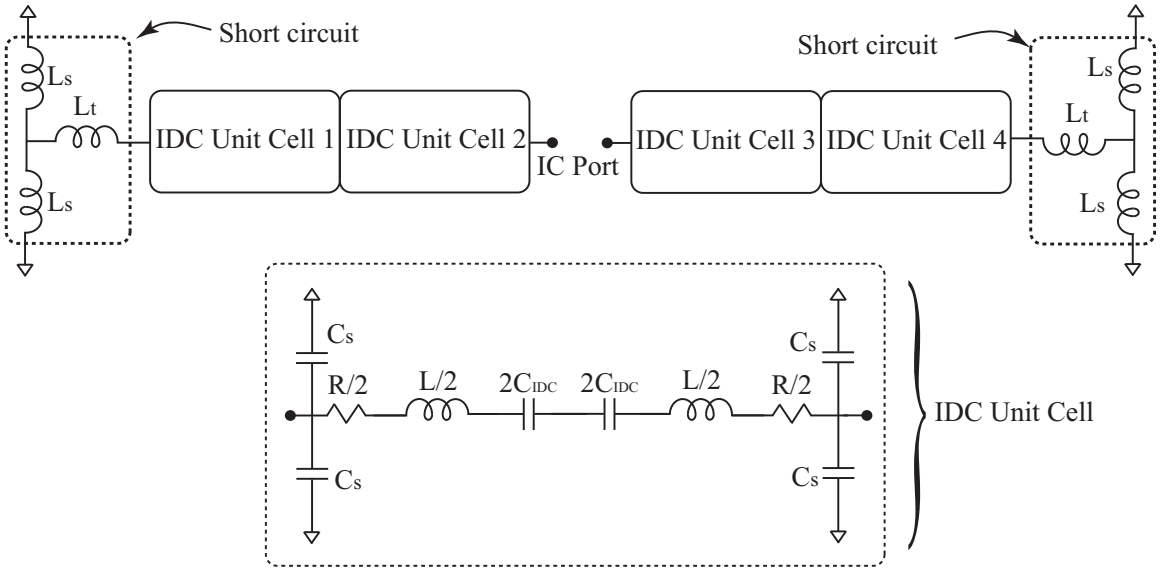

Figure 24. (a) Equivalent circuit of the proposed ZOR RFID antenna design II and (b) Equivalent circuit of an individual IDC unit-cell ($R = 0.68\ \Omega$, L = 3.04 nH, $C_{IDC} = 4.1$ pF, $C_s = 0.54$ pF, $L_s = 9.89$ nH and $L_t = 2.98$ nH).

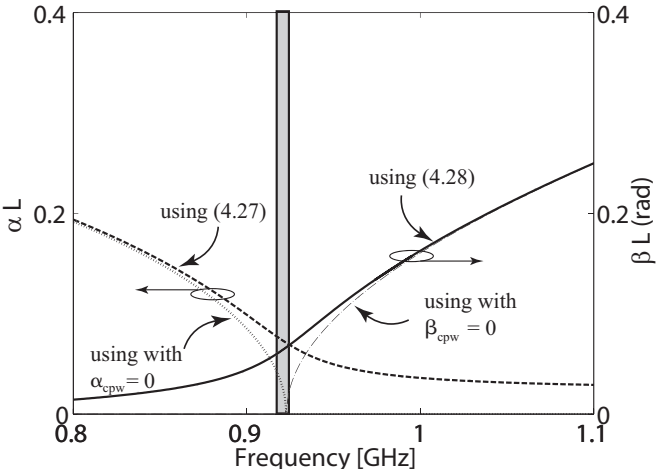

Figure 25. Dispersion diagrams of the lossy CPW IDC Unit-cell.

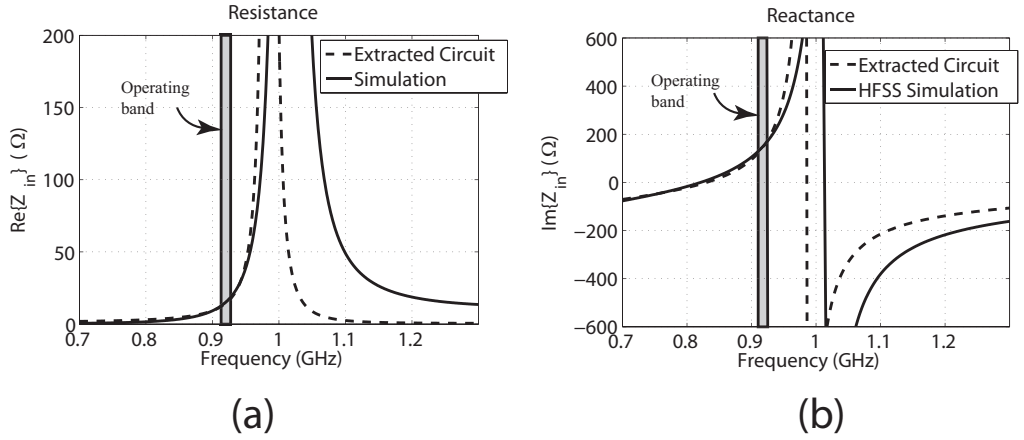

Figure 26. (a) Input resistance of the prototype antenna design II and (b) input reactance of the prototype antenna design II.

For comparison purpose a regular dipole antenna was designed with all the dimensions similar to the Design II except length of the arm. The prototype antenna is shown in Figure 28. The simulated resistance, reactance and return loss plots are shown in Figure 29 and Figure 30. From Figure 28, it can be noted that the design II is approximately 4.6 times smaller than equivalent dipole design.

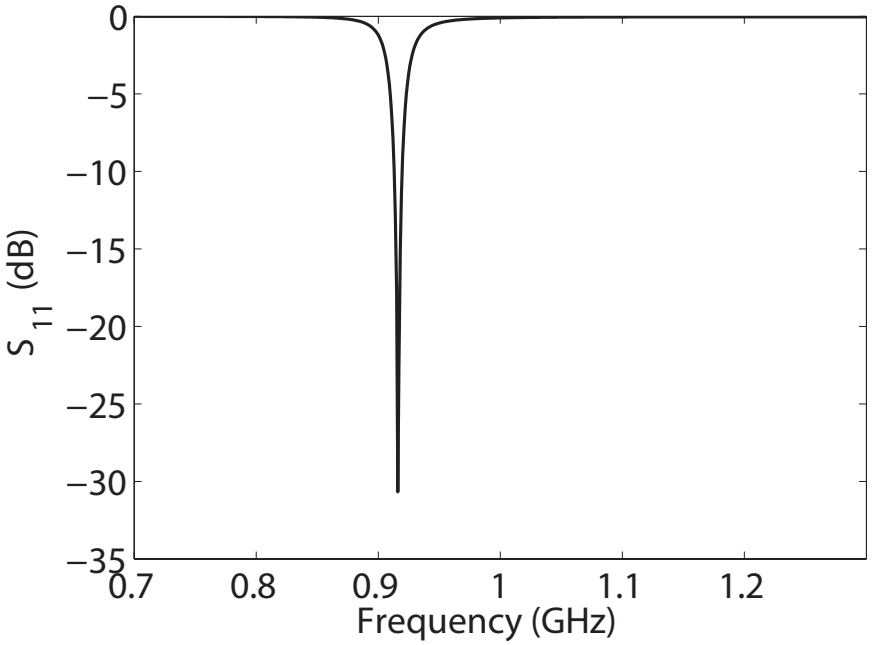

Figure 27. S_{11} of the prototype antenna design II.

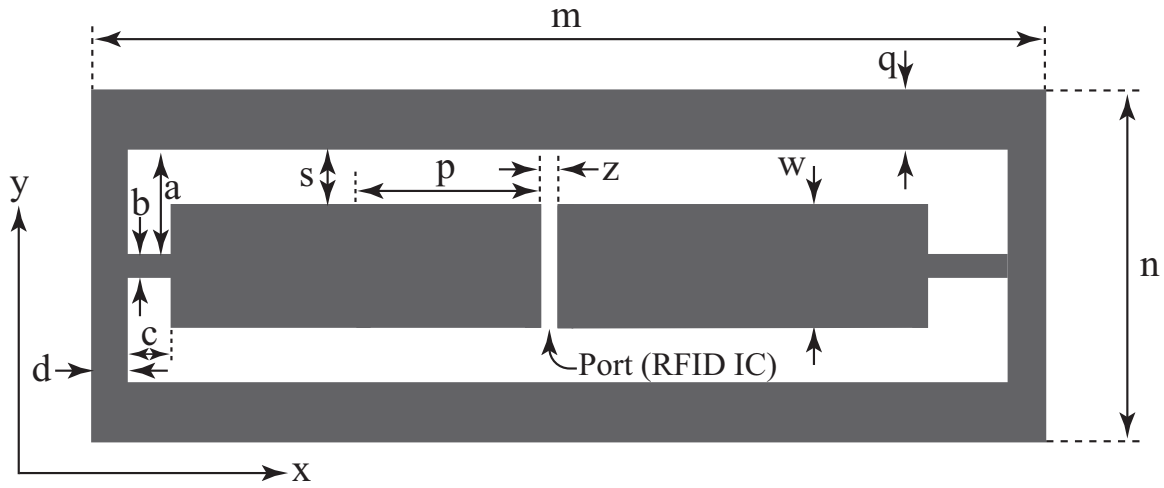

Figure 28. Layout of the regular dipole antenna for a passive UHF RFID tag with a = 16.3 mm, b = 0.6 mm, c = 3.5 mm, d = 1.0 mm, e = 0.6 mm, m = 271.6 mm, n = 44.8 mm, w = 15.2 mm, p = 12 mm, s = 9 mm, q = 5.8 mm, r = 3.5 mm, t = 1.0 mm, y = 1.0 mm and z = 1.0 mm.

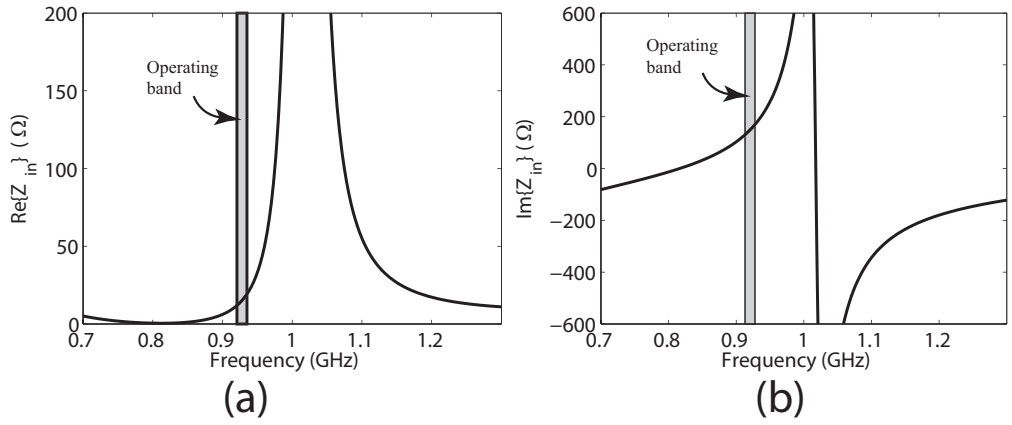

Figure 29. (a) Input resistance of the dipole prototype antenna and (b) input reactance of the dipole prototype antenna.

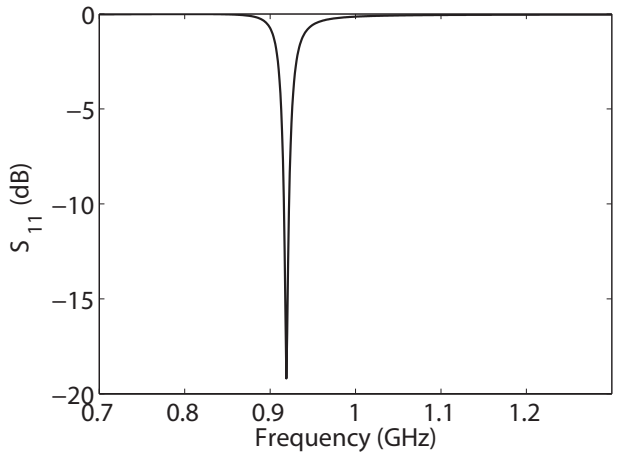

Figure 30. S_{11} of the dipole prototype antenna.

Next, to measure the read-range of the prototype RFID tag a similar set up was used as described in section 5.2. Because of the limited size of the chamber, a maximum read-range could not be determined by moving the tag away from the reader until it could no longer be read. The tag was placed at a distance of 2.5 m from the reader and an attenuation of 4 dB was added to just initiate the reading of the tag. Then using $R_{max} = 10^{\alpha_{dB}/20} R_{measured}$ [61] the predicted maximum read-range of 4 m was obtained.

5.4. Prototype Antenna Design III

The next step was to explore the shunt inductance based unit-cell shown in Figure 31. The proposed antenna shown in Figure 32 consists of six series connected shunt inductor unit-cells. The proposed antenna has an open circuit at both ends. The final dimensions were determined in HFSS to have a conjugate match at 920 MHz with the passive Higgs-2 RFID IC attached to the port. As with the IDC unit-cell, the antenna was simulated in HFSS on a Rogers TMM4 substrate with $\epsilon_r = 4.5$, $\tan\delta = 0.002$ and a substrate thickness $h = 1.524$ mm. The simulated input impedance and the return loss are shown in Figure 33 and Figure 34 respectively. Note that the input impedance ($Z_{in} = 15 + j145\Omega$) of the antenna is close to the conjugate value of the input impedance of the Higgs-2 IC ($Z_{IC} = 13.73 - j142.8\Omega$) at 920 MHz. The physical dimensions of the antenna are found to be $0.28\lambda_0 \times 0.09\lambda_0$. This means that an over all size reduction of about 11% is achieved with respect to the Design I.

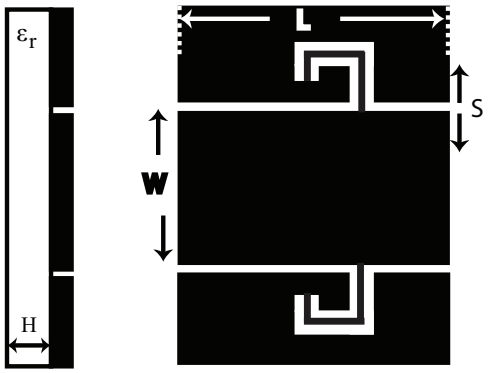

Figure 31. Shunt inductance loaded CPW unit-cell.

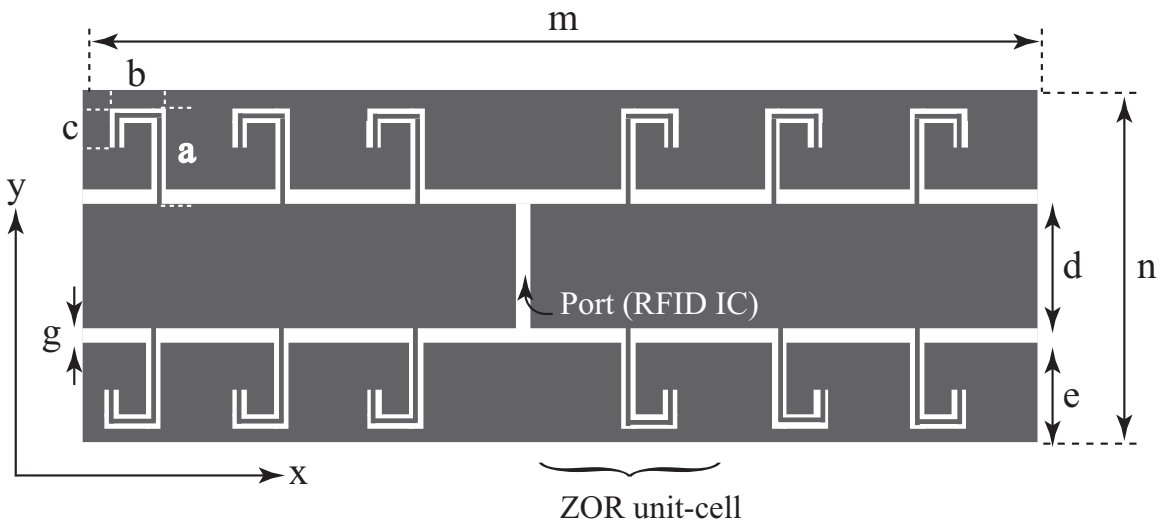

Figure 32. Layout of the ZOR antenna for a passive UHF RFID tag design III with a = 6 mm, b = 5.5 mm, c = 3.2 mm, d = 16.82, e = 6.8 mm, g = 0.4 mm, m = 91 mm, n = 31.22 mm and p = 15 mm.

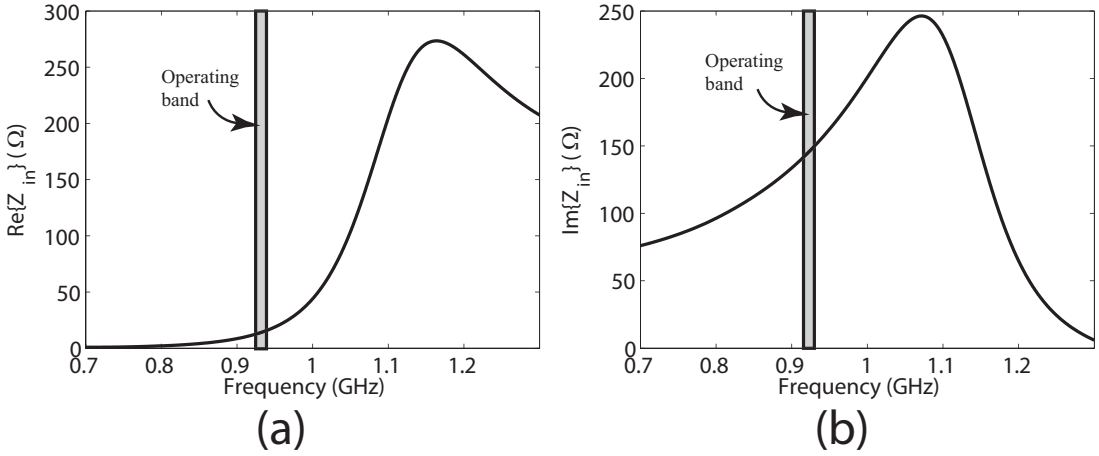

Figure 33. (a) Input resistance of the prototype antenna design III and (b) input reactance of the prototype antenna design III.

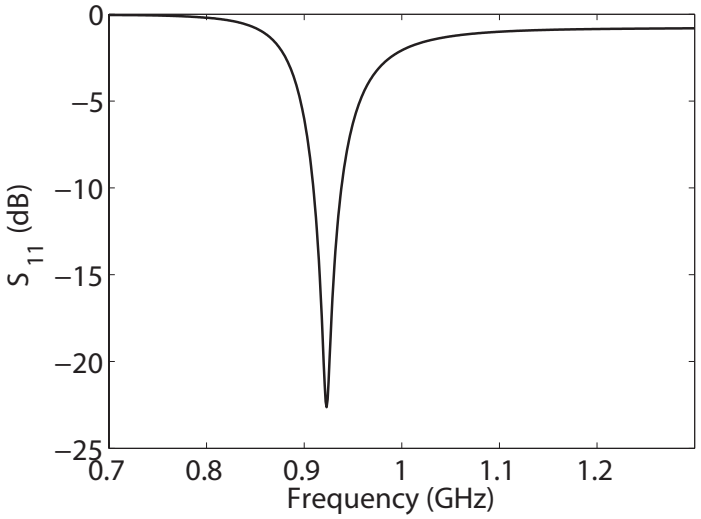

Figure 34. S_{11} of the prototype antenna design III.

Next, to measure the read-range of the prototype RFID tag similar set up was placed as described in section 5.2. Because of the limited size of the chamber, a maximum read-range could not be determined by moving the tag away from the reader until it could no longer be read. The tag was placed at a distance of 2.5 m from reader and attenuation of 7 dB is added to just initiate the reading of the tag. Then using $R_{max} = 10^{\alpha_{dB}/20} R_{measured}$ [61] the predicted maximum read-range of 5.5 m is obtained.

CHAPTER 6. CONCLUSION

In this work, a procedure for studying the zeroth order resonance using the interdigital capacitor and shunt inductor based CPW unit cells have been presented. Three novel antennas for passive UHF RFID tags have been proposed and developed. Two of these were based on inter-connected IDC unit-cells whereas one is based on shunt inductor unit-cells. The equivalent circuit models of IDC based passive UHF RFID antennas have been extracted, using the commercially available software ADS, resulting in a similar input impedance response as that of the layout version. The operating principle behind the RFID antenna depends on the zeroth order resonant (ZOR) frequency of the IDC unit-cell and shunt inductor unit-cell. Measurements have shown that the methodology presented in this work can be used to design an antenna on a prototype passive RFID tag with a good conjugate match to the passive IC. It was shown that predicted maximum read-range of 4.0 m, 5.5 m and even 7.6 m was possible with these antenna designs.

It is expected that this work will lay the foundation for future efforts in ZOR based RFID antenna design which can include unique and novel unit-cell designs to achieve smaller and compact sizes while maintaining similar ZOR frequencies. It is also anticipated that miniaturized ZOR based antenna arrays can be designed for a passive RFID tag for the first time. This will provide higher gain and thus longer read range values for a passive RFID tag.

BIBLIOGRAPHY

[1] K. Finkenzeller, *RFID Handbook: Fundamentals and Applications in Contactless Smart Cards and Identification.* NY, USA: John Wiley & Sons, Inc., 2 ed., 2003.

[2] Y.-C. Chen, M.-F. Hsieh, C.-C. Wang, and H.-R. Lee, "RFID-Based Intelligent Systems for Home-Healthcare," in *Digest of Technical Papers International Conference on Consumer Electronics (ICCE),* pp. 1 - 2, 2007.

[3] S. Manzari, C. Occhiuzzi, and G. Marrocco, "Feasibility of Body-Centric Systems Using Passive Textile RFID Tags," *IEEE Antennas and Propagation Magazine,* vol. 54, no. 4, pp. 49 - 62, 2012.

[4] P. Nikitin, K. V. S. Rao, and S. Lazar, "An Overview of Near Field UHF RFID," in *IEEE International Conference on RFID,* pp. 167 - 174, 2007.

[5] J. A. Paradiso, K.-y. Hsiao, and A. Benbasat, "Tangible music interfaces using passive magnetic tags," in *Proceedings of the 2001 conference on New interfaces for musical expression,* pp. 1 - 4, National University of Singapore, Singapore, 2001.

[6] R. Kanan and A. Azizi, "UHF RFID transponders antenna design for metal and wood surfaces," in *IEEE International Conference on RFID*, pp. 270 - 277, 2009.

[7] Teco:RFID Smart Shelf. [online] http://www.teco.edu/research/projects/smartshelf/.

[8] B. Braaten, M. Reich, and J. Glower, "A Compact Meander-Line UHF RFID Tag Antenna Loaded With Elements Found in Right/Left-Handed Coplanar Waveguide Structures," *IEEE Antennas and Wireless Propagation Letters,* vol. 8, pp. 1158 - 1161, 2009.

[9] A. Foroozesh and L. Shafai, "Size reduction of a microstrip antenna with dielectric superstrate using meta-materials: artificial magnetic conductors versus magneto-dielectrics," in *IEEE Antennas and Propagation Society International Symposium,* pp. 11 - 14, July 2006.

[10] B. Braaten and M. Aziz, "Using Meander Open Complementary Split Ring Resonator (MOCSRR) Particles to Design a Compact UHF RFID Tag Antenna," *IEEE Antennas and Wireless Propagation Letters,* vol. 9, pp. 1037 - 1040, 2010.

[11] V. G. Veselago, "The electrodynamics of substances with simultaneously negative values of ϵ and μ," *Physics-Uspekhi,* vol. 10, no. 4, pp. 509 - 514, 1968.

[12] G. Eleftheriades, A. Iyer, and P. Kremer, "Planar negative refractive index media using periodically L-C loaded transmission lines," *IEEE Transactions on Microwave Theory and Techniques,* vol. 50, pp. 2702 - 2712, Dec 2002.

[13] G. Eleftheriades, A. Grbic, and M. Antoniades, "Negative-refractive-index transmission-line metamaterials and enabling electromagnetic applications," in *IEEE Antennas and Propagation Society International Symposium,* vol. 2, pp. 1399 - 1402, June 2004.

[14] G. Eleftheriades, "Enabling RF/microwave devices using negative-refractive-index transmission-line (NRI-TL) metamaterials," *IEEE Antennas and Propagation Magazine,* vol. 49, pp. 34 - 51, April 2007.

[15] G. Eleftheriades, M. Antoniades, and F. Qureshi, "Antenna applications of negative-refractive-index transmission-line structures," *IET Microwaves, Antennas & Propagation,* vol. 1, pp. 12 - 22(10), February 2007.

[16] L. Brillouin, *Wave Propagation in Periodic Structures: Electric Filters and Crystal Lattices.* Dover phoenix editions, Dover Publications, 2003.

[17] V. Veselago, L. Braginsky, V. Shklover, and C. Hafner, "Negative Refractive Index Materials," *J. Comput. Theor. Nanosci.,* vol. 3, pp. 189 - 218, 2006.

[18] D. R. Smith, D. C. Vier, N. Kroll, and S. Schultz, "Direct calculation of permeability and permittivity for a left-handed metamaterial," *Applied Physics Letters,* vol. 77, no. 14, pp. 2246 - 2248, 2000.

[19] D. R. Smith, W. J. Padilla, D. C. Vier, S. C. Nemat-Nasser, and S. Schultz, "Composite Medium with Simultaneously Negative Permeability and Permittivity," *Phys. Rev. Lett.,* vol. 84, pp. 4184 - 4187, May 2000.

[20] D. R. Smith and N. Kroll, "Negative Refractive Index in Left-Handed Materials," *Phys. Rev. Lett.,* vol. 85, pp. 2933 - 2936, Oct 2000.

[21] F. Qureshi, M. Antoniades, and G. Eleftheriades, "A compact and low-profile metamaterial ring antenna with vertical polarization," *IEEE Antennas and Wireless Propagation Letters,* vol. 4, pp. 333 - 336, 2005.

[22] C.-J. Lee, K. M. K. H. Leong, and T. Itoh, "Broadband Small Antenna for Portable Wireless Application," in *International Workshop on Antenna Technology: Small Antennas and Novel Metamaterials (iWAT),* pp. 10 - 13, March 2008.

[23] J. Zhu and G. Eleftheriades, "A Compact Transmission-Line Metamaterial Antenna With Extended Bandwidth," *IEEE Antennas and Wireless Propagation Letters,* vol. 8, pp. 295 - 298, 2009.

[24] T. Jang, J. Choi, and S. Lim, "Compact Coplanar Waveguide (CPW)-Fed Zeroth-Order Resonant Antennas With Extended Bandwidth and High Efficiency on Vialess Single Layer," *IEEE Transactions on Antennas and Propagation,* vol. 59, pp. 363 - 372, Feb 2011.

[25] A. Sanada, M. Kimura, I. Awai, C. Caloz, and T. Itoh, "A planar zeroth-order resonator antenna using a left-handed transmission line," in *34th European Microwave Conference,* vol. 3, pp. 1341 - 1344, 2004.

[26] C.-J. Lee, K. M. K. H. Leong, and T. Itoh, "Composite right/left-handed transmission line based compact resonant antennas for RF module integration," *IEEE Transactions on Antennas and Propagation,* vol. 54, pp. 2283 - 2291, Aug 2006.

[27] J.-H. Park, Y.-H. Ryu, J.-G. Lee, and J.-H. Lee, "Epsilon Negative Zeroth-Order Resonator Antenna," *IEEE Transactions on Antennas and Propagation,* vol. 55, no. 12, pp. 3710 - 3712, 2007.

[28] B.-C. Park and J.-H. Lee, "Omnidirectional Circularly Polarized Antenna Utilizing Zeroth-Order Resonance of Epsilon Negative Transmission Line," I*EEE Transactions on Antennas and Propagation,* vol. 59, no. 7, pp. 2717 - 2721, 2011.

[29] C. Caloz and T. Itoh, *Electromagnetic metamaterials: transmission line theory and microwave applications.* John Wiley & Sons, 2005.

[30] L. Stutzman, Warren and A. Thiele, Gary, *Antenna Theory and Design.* New York: John Wiley & Sons, 2 ed., 1998.

[31] B. Braaten, G. Owen, D. Vaselaar, R. Nelson, C. Bauer-Reich, J. Glower, B. Morlock, M. Reich, and A. Reinholz, "A Printed Rampart-Line Antenna with a Dielectric Superstrate for UHF RFID Applications," in *IEEE International Conference on RFID,* pp. 74 - 80, 2008.

[32] K. V. S. Rao, P. Nikitin, and S. Lam, "Antenna design for UHF RFID tags: a review and a practical application," *IEEE Transactions on Antennas and Propagation,* vol. 53, no. 12, pp. 3870 - 3876, 2005.

[33] M. Stupf, R. Mittra, J. Yeo, and J. R. Mosig, "Some novel design for RFID antennas and their performance enhancement with metamaterials," *Microwave and Optical Technology Letters,* vol. 49, no. 4, pp. 858 - 867, 2007.

[34] B. Braaten, R. Scheeler, M. Reich, R. Nelson, C. Bauer-Reich, J. Glower, and G. Owen, "Compact Metamaterial-Based UHF RFID Antennas: Deformed Omega and Split-Ring Resonator Structures," *Applied Computational Electromagnetics Society Journal,* vol. 25, no. 6, pp. 530 - 542, 2010.

[35] J. Dacuna and R. Pous, "Miniaturized UHF tags based on metamaterials geometries Building Radio Frequency Identification for the Global Environment," [online] http://www.bridge-project.eu, july 2007.

[36] A. Sanada, C. Caloz, and T. Itoh, "Characteristics of the composite right/left-handed transmission lines," *IEEE Microwave and Wireless Components Letters,* vol. 14, no. 2, pp. 68 - 70, 2004.

[37] A. Rennings, T. Liebig, S. Abielmona, C. Caloz, and P. Waldow, "Tri-band and dual-polarized antenna based on composite right/left-handed transmission line," in *European Microwave Conference,* pp. 720 - 723, 2007.

[38] C.-J. Lee, K. Leong, and T. Itoh, "Compact Dual-Band Antenna Using an Anisotropic Metamaterial," in *36th European Microwave Conference,* pp. 1044 - 1047, 2006.

[39] S. Lim, C. Caloz, and T. Itoh, "Metamaterial-based electronically controlled transmission-line structure as a novel leaky-wave antenna with tunable radiation

angle and beamwidth," *IEEE Transactions on Microwave Theory and Techniques,* vol. 53, no. 1, pp. 161 - 173, 2005.

[40] J.-G. Lee and J.-H. Lee, "Zeroth Order Resonance Loop Antenna," *IEEE Transactions on Antennas and Propagation,* vol. 55, no. 3, pp. 994 - 997, 2007.

[41] A. Lai, K. Leong, and T. Itoh, "Infinite Wavelength Resonant Antennas With Monopolar Radiation Pattern Based on Periodic Structures," *IEEE Transactions on Antennas and Propagation,* vol. 55, no. 3, pp. 868 - 876, 2007.

[42] J. K. Ji, G.-H. Kim, and W. M. Seong, "A Compact Multiband Antenna Based on DNG ZOR for Wireless Mobile System," *IEEE Antennas and Wireless Propagation Letters,* vol. 8, pp. 920 - 923, 2009.

[43] S. Pyo, S.-M. Han, J.-W. Baik, and Y.-S. Kim, "A Slot-Loaded Composite Right/Left-Handed Transmission Line for a Zeroth-Order Resonant Antenna With Improved Efficiency," *IEEE Transactions on Microwave Theory and Techniques,* vol. 57, no. 11, pp. 2775 - 2782, 2009.

[44] J. Kim, G. Kim, W. Seong, and J. Choi, "A Tunable Internal Antenna With an Epsilon Negative Zeroth Order Resonator for DVB-H Service," *IEEE Transactions on Antennas and Propagation,* vol. 57, no. 12, pp. 4014 - 4017, 2009.

[45] J. K. Ji, G. H. Kim, and W. M. Seong, "Bandwidth Enhancement of Metamaterial Antennas Based on Composite Right/Left-Handed Transmission Line," *IEEE Antennas and Wireless Propagation Letters,* vol. 9, pp. 36 - 39, 2010.

[46] V. Sipal, A. Ajami, and D. Heberling, "Effect of Substrate Dimensions on Zeroth-Order Resonator Antennas," *IEEE Antennas and Wireless Propagation Letters,* vol. 9, pp. 107 - 109, 2010.

[47] C.-P. Lai, S.-C. Chiu, H.-J. Li, and S.-Y. Chen, "Zeroth-Order Resonator Antennas Using Inductor-Loaded and Capacitor-Loaded CPWs," *IEEE Transactions on Antennas and Propagation,* vol. 59, no. 9, pp. 3448 - 3453, 2011.

[48] S.-C. Chiu, C.-P. Lai, and S.-Y. Chen, "Compact CRLH CPW Antennas Using Novel Termination Circuits for Dual-Band Operation at Zeroth-Order Series and Shunt Resonances," *IEEE Transactions on Antennas and Propagation,* vol. 61, no. 3, pp. 1071 - 1080, 2013.

[49] C. Wen, "Coplanar Waveguide: A Surface Strip Transmission Line Suitable for Nonreciprocal Gyromagnetic Device Applications," *IEEE Transactions on Microwave Theory and Techniques,* vol. 17, no. 12, pp. 1087 - 1090, 1969.

[50] D. M. Pozar, *Microwave Engineering.* Hoboken, New Jersey: John Wiley & Sons, 3 ed., 2001.

[51] R. E. Collin, *Foundations for Microwave Engineering.* Hoboken, New Jersey: John Wiley & Sons, 2 ed., 2001.

[52] A. Velez, F. Aznar, J. Bonache, M. Velazquez-Ahumada, J. Martel, and F. Martin, "Open Complementary Split Ring Resonators (OCSRRs) and Their Application to Wideband CPW Band Pass Filters," *IEEE Microwave and Wireless Components Letters,* vol. 19, no. 4, pp. 197 - 199, 2009.

[53] G. V. Eleftheriates, and K. G. Balmain, *Negative-Refraction Metamaterials: Fundamentals Principles and Applications.* Hoboken, New Jersey: John Wiley & Sons, 2005.

[54] K.C. Gupta, R. Garg, and I.J. Bahl, *Microstrip Lines and Slotlines.* Massachusetts: Artech House, 1979.

[55] W. Hilberg, "From Approximations to Exact Relations for Characteristic Impedances," *IEEE Transactions on Microwave Theory and Techniques,* vol. 17, no. 5, pp. 259 - 265, 1969.

[56] A. Lai, T. Itoh, and C. Caloz, "Composite right/left-handed transmission line metamaterials," *IEEE Microwave Magazine,* vol. 5, no. 3, pp. 34 - 50, 2004.

[57] C. Caloz and T. Itoh, "Metamaterials for High-Frequency Electronics," *Proceedings of the IEEE,* vol. 93, no. 10, pp. 1744 - 1752, 2005.

[58] Ansoft HFSS Version 13.0.1, [online] http://www.ansoft.com.

[59] Alien Technologies, [online] http://www.alientechnologies.com.

[60] Agilent ADS 2009, [online] http://www.agilent.com.

[61] D. Vaselaar, "Passive UHF RFID design and utilization in the livestock industry," North Dakota State University, Fargo, U.S.A. 2008.